Research Square

Preprints are preliminary reports that have not undergone peer review.
They should not be considered conclusive, used to inform clinical practice,
or referenced by the media as validated information.

THC Exposure History Organizes Sex-Divergent Lipid Networks Across the Brain and Circulation

Chih-Yu Chen
Emory University School of Medicine, Emory Integrated Metabolomics and Lipidomics Core (EIMLC)
Laney Kimble
Medical University of South Carolina
Carolina Limbaker
Medical University of South Carolina
Kristal Maner-Smith
Emory University School of Medicine, Emory Integrated Metabolomics and Lipidomics Core (EIMLC)
Xueyun Gulbin
Emory University School of Medicine, Emory Integrated Metabolomics and Lipidomics Core (EIMLC)
Sung Ha Won
Emory University School of Medicine, Emory Integrated Metabolomics and Lipidomics Core (EIMLC)
Rachel Martin-Pendrod
Medical University of South Carolina
Onder Albayram
albayram@musc.edu

Medical University of South Carolina

Research Article

Keywords:

Posted Date: November 13th, 2026

DOI: https://doi.org/10.21203/rs.3.rs-11599512/v1

License: This work is licensed under a Creative Commons Attribution 4.0 International License.
Read Full License

Additional Declarations: No competing interests reported.

THC Exposure History Organizes Sex-Divergent Lipid Networks Across the Brain and Circulation

Chih-Yu Chen[1], Laney Kimble[2], Carolina Limbaker[2], Kristal Maner-Smith[1], Xueyun Gulbin[1], Sung Ha Won[1], Rachel Martin-Pendrod[2]†, Onder Albayram[2,3,4]†‡,

[1]Emory University School of Medicine, Emory Integrated Metabolomics and Lipidomics Core (EIMLC) Atlanta, GA, 30322, USA.

[2]Department of Neuroscience, Medical University of South Carolina, Charleston, SC, 29425, USA

[3]Department of Pathology and Laboratory Medicine, ER-AL Neurovascular Protection Laboratory, Medical University of South Carolina, Charleston, SC, 29425, USA

[4]Ralph H. Jackson Department of Veterans Affairs Medical Center, Charleston, SC, 29425, USA

† These authors jointly supervised this work.

‡ Corresponding Author

‡Corresponding Author

Onder Albayram, Ph.D.

Associate Professor

Department of Pathology and Laboratory Medicine

Department of Neuroscience

Medical University of South Carolina

Charleston, SC, USA

E-mail: albayram@musc.edu

Abstract:

Cannabis exposure is increasingly experienced as a dynamic and evolving history rather than as isolated episodes of intoxication, yet how prior Δ9-tetrahydrocannabinol (THC) exposure becomes biologically encoded across tissues remains largely unknown. Addressing this question is particularly important because adaptation to repeated cannabinoid exposure may involve coordinated metabolic remodeling that extends beyond transient pharmacological responses. Here, we integrated cannabinoid metabolite profiling with comprehensive brain and serum lipidomics to investigate how acute, repeated, and chronic THC vapor exposure across distinct life stages is associated with lipidomic states in the hippocampus and circulation of male and female rats. Rather than producing a uniform lipid response, THC exposure was associated with history-dependent lipidomic patterns and differential cannabinoid metabolite accumulation, including greater accumulation of 11-nor-9-carboxy-THC in females, alongside coordinated remodeling of membrane phospholipids, ether-linked phospholipids, sphingolipids, neutral lipids, and bioactive lipid mediators. These lipidomic trajectories differed by sex: females exhibited progressively broader and more persistent lipid remodeling across exposure histories, whereas males showed a predominantly acute hippocampal response. Although circulating lipid signatures partially paralleled hippocampal remodeling, brain and serum exhibited distinct yet coordinated metabolic programs, consistent with compartment-specific adaptation rather than a uniform lipidomic response. Systems-level network analyses further revealed sex-associated differences in lipid-network organization: females showed distributed, metabolite-integrated brain–serum lipid networks associated with sustained membrane remodeling, whereas males showed more module-centered networks organized around sphingolipid and ether-linked phospholipid programs. Together, these findings position exposure history as a biological variable associated with sex-dependent lipid-network organization, providing a systems framework for understanding how prior cannabinoid exposure is reflected in metabolic states across the brain and peripheral circulation.

Significance Statement:

Cannabinoid research has largely focused on individual exposure events, although cannabis use often follows repeated and evolving patterns across adulthood. How these exposure histories relate to longer-term metabolic organization remains poorly understood. By integrating cannabinoid metabolite profiling with hippocampal and serum lipidomics, we identify sex-dependent patterns of lipid remodeling and brain–serum network coordination across distinct THC exposure histories. Females exhibited more persistent hippocampal lipid alterations and distributed metabolite-associated networks, whereas males showed a predominantly acute hippocampal response and more module-centered brain–serum coordination. These findings highlight exposure history and biological sex as important dimensions of cannabinoid-associated metabolic organization, providing a framework for investigating the longer-term biological consequences of repeated THC exposure.

Introduction:

Cannabis use often follows evolving trajectories across adulthood, encompassing early experimentation, intermittent re-exposure, and sustained or recurrent use (1). Yet whether such exposure histories leave persistent metabolic signatures, and how these signatures differ across tissues, remains poorly understood. Δ9-Tetrahydrocannabinol (THC), the principal psychoactive constituent of cannabis, is highly lipophilic, distributes extensively across tissues, and undergoes metabolism to 11-hydroxy-THC and 11-nor-9-carboxy-THC through pathways involving CYP2C9, CYP2C19, and CYP3A enzymes (2, 3). Together, these properties raise the possibility that repeated THC exposure across distinct life stages may be associated with metabolic changes extending beyond transient cannabinoid receptor signaling.

Whether THC exposure history is reflected in similar biological responses in females and males remains an equally important question. Human and preclinical studies indicate that biological sex influences cannabinoid sensitivity, pharmacokinetics, tissue distribution, metabolism, and behavioral responses (4-6). Rodent studies further reveal age- and sex-dependent differences in THC disposition, suggesting that parent THC, 11-hydroxy-THC, and 11-nor-9-carboxy-THC may reflect distinct aspects of cannabinoid exposure and metabolism across life stages (5-7). Because tissue-specific cannabinoid metabolism and enzymatic activity were not directly measured, differences in metabolite abundance cannot establish the mechanisms underlying these sex-dependent profiles. Whether these sex-dependent metabolite profiles are associated with distinct patterns of metabolic remodeling remains unclear.

The lipidome provides a compelling framework for investigating these relationships, given the close integration of cannabinoid signaling with membrane lipid metabolism. Endocannabinoids and related N-acylethanolamines arise from membrane-associated lipid pathways and are closely linked to phospholipid, lysophospholipid, and monoacylglycerol metabolism (8-11). Ether-linked phospholipids, including ethanolamine plasmalogens, contribute to membrane organization, vesicular function, cellular signaling, and protection against oxidative stress (12, 13). Sphingolipids and glycosphingolipids contribute to membrane-domain organization and stress signaling, whereas triglycerides and other neutral lipids participate in systemic lipid transport and storage (14, 15). Together, these lipid classes form interconnected structural, signaling, and metabolic systems that support cellular homeostasis and responses to physiological perturbation (11, 15). Thus, the metabolic signatures associated with THC exposure history may extend beyond changes in individual lipid species to coordinated patterns of lipid-network organization.

Whether THC exposure history is associated with coordinated lipid remodeling across the brain and peripheral circulation, or with compartment-specific responses, remains unclear. The hippocampus is a cannabinoid-sensitive region in which membrane lipid composition, synaptic signaling, and metabolic homeostasis are closely linked, whereas serum reflects systemic lipid

transport, peripheral metabolism, and circulating lipid homeostasis (15, 16). Although circulating lipid signatures may share features with central lipid remodeling, they also reflect peripheral metabolic processes and cannot be assumed to represent the brain lipidome directly (15, 16). Integrating hippocampal and serum lipidomics may therefore reveal both shared and compartment-specific patterns associated with THC exposure history, while distinguishing coordinated lipid variation from direct evidence of metabolic exchange.

Here, we used a life-stage-resolved THC vapor paradigm to investigate how acute, repeated, and chronic exposure histories are associated with cannabinoid-metabolite profiles and lipidomic remodeling across the hippocampus and circulation in female and male rats. By combining targeted cannabinoid-metabolite quantification with untargeted and targeted lipidomics and integrative network analyses, we examined lipid remodeling from individual molecular species to coordinated brain–serum modules. We asked whether lipidomic patterns differed by exposure history and sex, and whether hippocampal and circulating lipid programs exhibited shared or compartment-specific organization. Across these analyses, females exhibited increasingly extensive and persistent hippocampal lipid remodeling, accompanied by distributed metabolite–lipid network associations, whereas males showed a predominantly acute hippocampal response and more module-centered brain–serum coordination. Together, these findings suggest that THC exposure history and biological sex are associated with distinct patterns of lipid-network organization across central and circulating metabolic compartments.

Methods:

Animals

All animal procedures were approved by the Medical University of South Carolina Institutional Animal Care and Use Committee (IACUC). Male and female Sprague–Dawley rats were obtained from Envigo (Indianapolis, IN, USA) at 3–5 weeks of age. Animals were pair-housed under a reversed 12-h light/12-h dark cycle in a temperature- and humidity-controlled vivarium. Each experimental group (acute THC, repeated THC, chronic THC, and repeated vehicle) comprised eight males and eight females. Animals in the acute and repeated exposure groups had ad libitum access to food and water throughout the study. In contrast, animals in the chronic THC group underwent food restriction from approximately 20 to 37 weeks of age and were subsequently provided primarily a low-fat diet ad libitum from approximately 37 weeks of age until euthanasia at 62 weeks. All animals were acclimated to the facility for at least 5 days before the initiation of vapor exposure.

Vapor Exposure

Rats underwent vapor exposure during predefined developmental stages according to their assigned exposure history. The chronic THC group received 20 exposure sessions during adolescence (postnatal days [PD] 39–63), adulthood (PD 108–133), and late adulthood (PD 409–434), for a total

of 60 sessions. The repeated THC group received 20 sessions during adolescence (PD 30–55) and adulthood (PD 107–132), for a total of 40 sessions. The repeated vehicle group followed a comparable schedule during adolescence (PD 33–60) and adulthood (PD 108–133), receiving 40 vehicle exposure sessions. The acute THC group received 20 sessions during adolescence (PD 31–46). Sessions were conducted daily, excluding weekends.

For THC exposure, rats were administered vapor generated from a 100 mg/mL cannabis extract solution (~70% THC, low CBD; NIDA Drug Supply Program) prepared in 90% propylene glycol and 10% vegetable glycerin. Vehicle exposure used the same solvent mixture without cannabis extract. Vapor was delivered using an eight-chamber apparatus equipped for passive and self-administration. Cannabis extract or vehicle solution was loaded into atomizers (Geekvape Z-series subohm tanks), and vapor was generated and delivered into the chambers. A vacuum pump connected to an inline filter and liquid scavenger facilitated vapor delivery and removal.

Tissue Collection and Euthanasia

All animals were euthanized by rapid decapitation without anesthesia immediately following their final vapor exposure session. Trunk blood was collected into 10-mL BD Vacutainer tubes, allowed to clot at room temperature, and centrifuged at maximum relative centrifugal force (RCF) for 10 min at 4°C. Serum was transferred into 1.5-mL microcentrifuge tubes and stored at −80°C until analysis. Brains were rapidly extracted and hemisected. The hippocampus was dissected from the medial surface of one hemisphere, transferred into a 1.5-mL microcentrifuge tube, flash-frozen in 2-methylbutane, and stored at −80°C. The contralateral hemisphere was wrapped in aluminum foil, flash-frozen in 2-methylbutane, and stored at −80°C.

Untargeted lipidomics

Untargeted, high resolution lipidomics was performed on rat serum and brain samples according to the manufacturer's recommended protocols. Briefly, pooled quality control (QC) samples were prepared for each matrix by combining 10 µl aliquots of each individual serum sample or of each homogenized brain sample. Lipids were extracted from 50 µl serum/50 mg brain/QC samples using a high-throughput monophasic methyl *tert*-butyl ether (MtBE)-based method on an automated sample preparation system (Biotage Extrahera, Uppsala, Sweden). Serum samples were spiked with 10 µl internal standard (Splash Lipidomix, Avanti Polar Lipids, Alabaster, AL) and 200 µl methanol containing 50 µg/ml BHT to precipitate proteins, centrifuged, and the supernatant filtered through a 0.25 µm PTFE filter plate. Lipids were subsequently eluted with MtBE:methanol (3:1, v/v) followed by 100% MtBE, dried under nitrogen, and reconstituted in 200 µl acetonitrile:isopropanol (1:1, v/v) for LC-MS analysis. Lipid separation was performed on a 1290 Infinity II LC system (Agilent, Santa Clara, CA) using an Accucore C18 column (100 x 4.6 mm) with a 25-min gradient of ammonium formate-buffered acetonitrile/isopropanol solvents at 55°C and a flow rate of 0.5 ml/min. Eluted lipids were

analyzed on a TIMS TOF Pro 2 mass spectrometer (Bruker Daltonics, Bremen, Germany) equipped with a VIP-HESI source in both positive and negative ionization modes using DDA-PASEF acquisition. Instrument parameters were optimized using internal standards and maintained throughout the analysis, and QC samples were injected at the beginning and end of the analytical run and after every 10 serum samples to monitor instrument stability and analytical reproducibility. Raw data were processed in MetaboScape 2024b (Bruker Daltonics) for peak detection, alignment, and lipid annotation using the T-Rex 4D algorithm based on m/z, MS/MS spectra, and collisional cross-section values (The MS/MS confidence criteria were listed in **Table S1**.). Annotated lipids were filtered using intensity, blank, and QC criteria. Features with a mean sample intensity < 1000 were excluded. Lipids were retained if the ratio of sample maximum intensity to mean blank intensity > 10, and the ratio of mean QC intensity to mean blank intensity > 3. Additionally, lipids with a QC CV greater than 150% were removed. For de-duplication, lipids detected in both positive and negative ionization modes were retained as separate entries. When multiple adducts were annotated for the same lipid species, only the predominant adduct was kept following manual review. A total of 871 and 842 lipids were detected in serum and brain samples, respectively. The annotated lipid list was provided in **Table S2** (brain) and **S3** (serum). The parameters of chromatography and MS spectrometry were detailed in **Tables S4** and **S5**.

Targeted lipidomics

Oxylipins and endocannabinoids were quantified by external calibration using analytical-grade standards, all purchased from Cayman Chemical (Ann Arbor, MI). The endocannabinoid and N-acylethanolamine standards were prostaglandin E2 ethanolamide (PGE2-EA), oleoyl ethanolamide (OEA), palmitoyl ethanolamide (PEA), arachidonoyl ethanolamide (AEA), docosahexaenoyl ethanolamide (DHEA), linoleoyl ethanolamide (LEA), stearoyl ethanolamide (ceramid; SEA), oxy-arachidonoyl ethanolamide (oxy-AEA), 2-arachidonoyl glycerol (2-AG), docosatetraenoyl ethanolamide (DEA), α-linolenoyl ethanolamide (ALEA), oleamide, dihomo-γ-linolenoyl ethanolamide (DGLEA), and docosanoyl ethanolamide. The oxylipin standards were prostaglandin E2-1-glyceryl ester (prostaglandin), prostaglandin E2 (PGE2), 9,10-dihydroxy-12Z-octadecenoic acid (9,10-DiHOME), 20-hydroxyeicosatetraenoic acid (20-HETE), 9-HETE, 5(S)-HETE, 12(R)-HETE, 14,15-dihydroxyeicosatrienoic acid (14,15-DiHET), 11(12)-DiHET, 5,6-DiHET, 8(9)-DiHET, thromboxane B2 (TXB2), 12(13)-epoxyoctadecenoic acid (12(13)-EpOME), 13-hydroxyoctadecadienoic acid (13-HODE), 9(S)-HODE, prostaglandin F2α (PGF2α), 8-iso-prostaglandin F2α (8-iso-PGF2α; 8-isoprostane), 14(15)-epoxyeicosatrienoic acid (14(15)-EET), 8(9)-EET, 11(12)-EET, leukotriene B4 (LTB4), 13-oxo-octadecadienoic acid (13-KODE), 13(S)-hydroperoxyoctadecadienoic acid (13(S)-HpODE), 9(S)-HpODE, 9(S)-hydroxyoctadecatrienoic acid (9(S)-HOTrE), 13(S)-HOTrE, resolvin D1 (RvD1), RvD2, RvD3, RvE1, maresin 1 (MaR1), and MaR2. THC and its metabolites, (-)-11-Nor-9-carboxy-delta-THC, 11-Hydroxyl-delta9-THC, and (-)-delta9-THC were obtained from [company].

Calibration curves were prepared of these standards over the linear range of 0.1-10 nM and the equation of the slope used for quantification of the corresponding lipid in the serum and brain samples. Oxylipins and THC were isolated from serum and brain samples using an automated C18 solid phase extraction manifold, the Biotage Extrahera (Biotage, Uppsala, Sweden). Samples were first homogenized with 3 times the volume of cold PBS buffer, then diluted by 3x sample volume of 20% methanol with 0.1% BHT. Finally, the pH of the samples was adjusted to 3.0 by the addition of 80µl of glacial acetic acid. Samples were centrifuged then at 4000 rpm for 15 min at 4˚C to pellet any precipitated solids. The supernatant was transferred to a preconditioned C18 SPE plate (Isolute C18, Biotage, Uppsala, Sweden). The sample was rinsed with 800 µl water, followed by 800µl hexane. The oxylipins were then eluted off of the SPE column with 400 µl methyl formate. The recovered oxylipin fraction was then dried under nitrogen gas and subsequently reconstituted in methanol to be analyzed by LC/MS. Extracted lipids were resolved using an Infinity II/6495C LC/MS system (Agilent, Santa Clara, CA). To quantify the oxylipins in extract, 6µl sample was injected onto an Accucore C18 column (100 x 4.6 mm, Thermo, Waltham, MA) and resolved on a 25-min gradient using water as Solvent A and acetonitrile as Solvent B, both contain 10 mM ammonium acetate. The column was heated to 35°C in a temperature-controlled column chamber and 0.4-0.5 ml/min flow rate was used for analysis. The gradient used for analysis was listed in **Table S6**. Eluted oxylipins and endocannabinoids were analyzed by an Agilent 6495C (Agilent, Santa Clara, CA) mass spectrometer operated in both negative and positive ion modes, respectively, using the instrument's rapid polarity switching capabilities. Instrumental parameters were optimized using external analytical grade standards and were held consistent over the course of analysis. Instrumental parameters were listed in **Table S7**. Oxylipins were analyzed in the negative ion mode while endocannabinoids were analyzed in the positive ion mode; both classes of lipids were targeted using a multiple reaction monitored (MRM) based method. For this, the mass of the target lipid and a characteristic fragment were used for detection. Oxylipins, endocannabinoids, and THC analytes were measured using a targeted MRM panel of 49 analytes (**Table S8**), of which 17 lipid mediators in brain and 23 in serum were detected and retained for analysis (**Tables S9** and **S10**). Raw data for analytical grade standards and samples were uploaded into an open source software, Skyline, for peak integration. To quantify oxylipins and endocannabinoids, the area under the curve of each identified lipid was calibrated against an external calibration curve. To create the curve, analytical grade standards in the linear range of 0.1 nM-10 nM were created for each standard. The lower limits of detection and upper limits of detection were determined, plotting concentration versus area under the curve. The slope of the linear regression equation was used for calibration of the corresponding analyte. The resulting sample concentrations were reported as ng/µl for serum and ng/mg of tissue for brain.

Data Processing and Covariate adjustment

Untargeted and targeted lipidomics data were first normalized to total lipid abundance. For brain samples, lipid intensities were additionally normalized by tissue weight, while for serum samples they were normalized by sample volume. After normalization, missing values were imputed on a per-feature basis using half of the minimum observed value, and the resulting data were log2-transformed prior to covariate adjustment. To account for age-related variation, the association between each feature and rat age was assessed using linear modeling. Age effects were subsequently removed using the removeBatchEffect() function in limma R package (17), specifying age as a continuous covariate while preserving the primary biological variable of interest (sex) in the design matrix. This procedure removes the linear contribution of age from each feature while retaining biologically relevant variation associated with sex (**Fig. S1B-E**). Because exposure history was aligned with life stage, this adjustment cannot separate age-dependent from exposure-dependent effects; as a sensitivity analysis, differential analyses were therefore repeated on log2-transformed data without age adjustment (**Fig. S12, S13**). Following age adjustment, data from targeted and untargeted lipidomics were jointly analyzed. To minimize differences in signal scale and distribution between datasets, the age-adjusted data were further normalized using feature- and sample-centering. Feature centering was applied to emphasize relative variation in each lipid across samples, while sample centering reduced global intensity differences between samples. This normalization facilitated integrative analyses across platforms by minimizing platform-dependent effects while preserving biologically meaningful variation. The resulting data were used for downstream statistical analyses. PCA was performed for outlier detection and quality control. Four samples with ~50% missingness clustered separately from the remaining samples and were therefore removed prior to downstream analyses.

Differential abundance analysis

Differential abundance analysis was performed using both untargeted and targeted lipidomics datasets. To identify individual lipids altered by THC exposure, linear models were fitted using the limma package (limma::lmFit), followed by empirical Bayes variance shrinkage (limma::eBayes). DE analyses were performed for each contrast (THC vs vehicle) across exposure durations (acute, repeated, and chronic) in brain lipidomics, and for exposure-based comparisons in both brain and serum datasets, stratified by sex. Statistical significance ($p < 0.05$) and log fold changes were visualized using volcano plots and UpSet plots. The results are listed in **Table S9** and **S10**. Results without age adjustment are shown in **Fig. S12**.

Weighted correlation network analysis

Weighted correlation network analysis (WGCNA) was performed using the WGCNA package (18) to identify consensus modules shared between female and male datasets, following the same framework used for the lipid network analysis. Soft-thresholding powers were selected to approximate scale-free topology: $\beta = 12$ for brain lipidomics (scale-free fit, $R^2 = 0.949$ in males and 0.973 in females) and $\beta =$

10 for serum lipidomics (scale-free fit, $R^2 = 0.903$ in males and 0.877 in females). A signed consensus network was constructed by computing component-wise consensus topological overlap matrices (TOMs) across the female and male datasets. Lipid features were clustered by average-linkage hierarchical clustering using consensus dissimilarity (1 − TOM). Modules were defined using Dynamic Tree Cut (deepSplit = 4, cutHeight = 0.995, pamRespectsDendro = FALSE; minimum module size = 25 for brain and 30 for serum), and closely related modules were merged at a cut height of 0.20 (eigengene correlation ≥ 0.80). Consensus module eigengenes (MEs) were calculated to summarize the abundance patterns of lipids within each module. In total, 10 consensus lipid modules were identified in brain and 12 in serum. Module eigengenes were subsequently used for association analyses with phenotypes (THC levels) using Pearson correlation. Figures S6 and S7 summarize the WGCNA workflow and key network characteristics for the brain and serum lipidomics datasets, respectively. Consensus module membership (MM), corresponding P values, and module assignments for individual lipids are provided in **Table S11** (brain) and **Table S12** (serum).

Multivariate integration

Multivariate integration was performed at the lipid-feature and WGCNA-module levels using the same two-step strategy. First, discriminative variables were identified within each data block by stability selection using multinomial elastic-net regression (glmnet (19); $\alpha = 0.5$). Variables were standardized before model fitting, and the regularization parameter was set to lambda.1se based on four-fold cross-validation. Selection was repeated across 200 stratified bootstrap resamples, and variables with non-zero coefficients in ≥60% of resamples were retained. Second, the stability-selected variables were integrated using DIABLO (block.splsda, mixOmics R package (20)) with two components and an off-diagonal design value of 0.1, prioritizing discrimination among groups over between-block covariance. Because variable selection was performed upstream, all stability-selected variables were retained in the DIABLO model without additional feature selection. Samples were visualized using the average of the block-specific component scores, with equal contribution from each block.

For feature-level integration, untargeted and targeted lipidomics datasets were treated as separate data blocks, and models were fitted separately for brain and serum. The response variable encoded combined exposure-by-sex groups: four groups for the age-matched brain comparison (repeated vehicle and repeated THC in each sex; **Fig. 1C**), eight groups for the brain exposure-history analysis (vehicle, acute, repeated, and chronic exposure in each sex; **Fig. 2B**), and six groups for the serum exposure-history analysis (acute, repeated, and chronic exposure in each sex; **Fig. S4C**). For module-level integration, WGCNA-derived module eigengenes (MEs) from brain and serum were treated as separate data blocks, providing reduced-dimensional summaries of coordinated lipidomic variation within each tissue. Because serum was not collected from vehicle-treated animals, the module-level analysis was restricted to acute, repeated, and chronic exposure groups with matched brain and serum samples, resulting in six exposure-by-sex groups (**Fig. 4D; Fig. S8D**).

Overrepresentation analysis in modules

To determine which lipid classes were enriched within each WGCNA module, we performed overrepresentation analysis (ORA) using one-sided Fisher's exact tests, with all annotated lipids serving as the background universe. Hub lipids were defined as those with high module membership (MM > 0.6 and $p < 0.05$). For each lipid class, the number of lipids present in the hub lipid set (query) and the full lipid background (universe) was tabulated, and enrichment was assessed using one-sided Fisher's exact tests. For each class, the proportion of lipids in the query and background was calculated, and fold enrichment was defined as the ratio of % query to % background. Raw p values were adjusted using the q value method (False discovery rate, FDR), and lipid classes with FDR q values < 0.05 were considered significantly enriched.

Lipid set enrichment analysis

Lipid set enrichment analysis (LSEA) was conducted using a rank-based method analogous to gene set enrichment analysis (GSEA), implemented in the fgsea R package (21). DE results for individual lipids were used to generate ranked lists for each contrast, and enrichment was evaluated separately by tissue. For brain lipidomics (which included a vehicle (Veh) group), contrasts comprised within-sex comparisons among THC exposure conditions (Repeated vs Acute, Chronic vs Acute, Chronic vs Repeated) as well as comparisons versus Veh (Acute vs Veh, Repeated vs Veh, Chronic vs Veh). For serum lipidomics (no vehicle group), contrasts were restricted to within-sex comparisons among exposure conditions (Repeated vs Acute, Chronic vs Acute, Chronic vs Repeated). In both tissues, sex comparisons were additionally evaluated within each exposure condition (Male vs Female within Acute, Repeated, Chronic, or Veh (brain only)). For each contrast, lipids were ranked by the DE ranking metric (e.g., signed test statistic), and LSEA was used to test whether predefined lipid classes were overrepresented at the extremes of the ranked list. Enrichment analysis was conducted using the fgsea R package, restricting lipid classes to a minimum size of 10. 10000 permutations were used to estimate nominal p-values and to compute normalized enrichment scores (NES). Lipid classes with raw $p < 0.05$ were considered significantly enriched for a given contrast. Results were listed in **Table S13** and **S14**.

Other Statistical analysis

All statistical analyses were performed in RStudio (R version 4.5.0). THC analyte concentrations were compared by two-way ANOVA (exposure group × sex) followed by Tukey's HSD post hoc test. Summed lipid-class abundances and ratios were compared across exposure groups within each sex by one-way ANOVA. For comparisons of module eigengene (ME) values, non-parametric Kruskal-Wallis tests were applied. Data visualization was performed using the ggplot2, ComplexHeatmap, ComplexUpset, ggh4x, pheatmap, circlize, tidygraph, and igraph R packages.

Results:

Repeated THC Vapor Exposure Reveals Sex-Divergent Brain Cannabinoid Metabolite Profiles and Lipidomic Organization.

We first used a controlled THC vapor exposure paradigm to examine cannabinoid accumulation and brain lipidomic organization across sexes. Male and female rats underwent acute, repeated, or chronic THC exposure histories, with a repeated vehicle group matched to the repeated THC group for vapor procedures, handling, and age at tissue collection (**Fig. 1A**). Each exposure epoch comprised 20 sessions, with five trials per session and two 3-s puffs of 100 mg/mL cannabis extract (~70% THC) per trial. The acute group received a single exposure epoch during adolescence, the repeated group received additional exposure during adulthood, and the chronic group underwent a third epoch in later adulthood. The repeated THC–vehicle comparison provided the principal age-matched control for evaluating THC-associated biochemical changes.

Untargeted lipidomics revealed distinct lipid-class distributions across brain and serum (**Fig. S1A**). Brain lipids were enriched in ether-linked phospholipids (O-PL, 16.15%), phosphatidylcholines (PC, 15.63%), and hexosylceramides (HexCer, 14.21%), whereas serum contained higher proportions of triacylglycerols (TG, 22.63%), PC (21.30%), and O-PL (10.36%). These profiles established the differing lipid compositions of the central and circulating compartments examined in this study.

We next quantified brain Δ9-THC and its major metabolites in the controlled repeated-exposure comparison (**Fig. 1B**). In females, repeated THC exposure significantly increased Δ9-THC ($p = 0.0335$), 11-hydroxy-Δ9-THC (H-Δ9-THC; $p = 0.0467$), and 11-nor-9-carboxy-Δ9-THC (C-Δ9-THC; $p = 0.0001$) relative to vehicle. In males, Δ9-THC ($p = 0.046$) and H-Δ9-THC ($p = 0.0131$) were significantly elevated, whereas C-Δ9-THC remained low and showed no comparable increase. Cannabinoid analytes were negligible or near analytical background in retained vehicle samples following quality-control review. Thus, repeated THC exposure produced measurable brain cannabinoid accumulation in both sexes, with a distinct female-associated profile characterized by greater C-Δ9-THC abundance.

We then examined whether these cannabinoid profiles were accompanied by differences in brain lipidomic organization. Integrated untargeted and targeted lipidomics revealed exposure- and sex-associated multivariate structure (**Fig. 1C**). Unsupervised principal component analysis (PCA) showed partial group organization, with PC1 and PC2 explaining 30% and 15% of total variance, respectively. Multiblock partial least squares discriminant analysis (PLS-DA) further distinguished repeated THC from vehicle samples primarily along averaged variate 1, with additional sex-associated structure along averaged variate 2. These findings indicate that repeated THC exposure and biological sex contributed to distinct patterns of brain lipidomic variation.

Features contributing to multivariate discrimination spanned structural membrane lipids and bioactive mediators (**Fig. 1D, E**). In untargeted lipidomics, phosphatidylethanolamine (PE),

phosphatidylserine (PS), PC, sphingomyelin (SM), HexCer/SHexCer-related glycosphingolipids, and lysophosphatidylethanolamine (LPE) species contributed prominently to the first two components (**Fig. 1D**). Targeted lipidomics identified PGE2, PEA, 9-HETE, DEA, and 13-HODE among the discriminant bioactive mediators (**Fig. 1E**). Thus, exposure-associated lipidomic variation involved multiple membrane lipid classes together with selected oxylipins and N-acylethanolamine-related mediators.

Finally, we examined correlations between selected brain lipid features and individual cannabinoid analytes (**Fig. 1F**). Phospholipids, lysophospholipids, sphingolipids, and bioactive mediators exhibited both positive and inverse associations with Δ9-THC, H-Δ9-THC, and C-Δ9-THC. Notably, DEA and SM 41:7;O3 were inversely associated with Δ9-THC and H-Δ9-THC. These relationships indicate that lipidomic variation was associated with distinct cannabinoid analytes rather than a single uniform THC-related pattern. Together, the controlled repeated-exposure comparison revealed sex-associated differences in brain cannabinoid metabolite profiles alongside coordinated variation in membrane lipids and bioactive mediators, providing a foundation for examining lipidomic remodeling across extended THC exposure histories.

THC Exposure Histories Reveal Sex-Divergent Hippocampal Lipid Remodeling and Persistence.

Building on the controlled repeated-exposure comparison, we next examined how hippocampal cannabinoid burden and lipidomic remodeling varied across acute, repeated, and chronic THC exposure histories. These regimens represented successive exposure epochs across adolescence, adulthood, and later adulthood rather than conventional dose-response conditions. The repeated vehicle group served as the principal procedural reference, while age-associated lipid variation was evaluated through adjusted and unadjusted analyses.

Hippocampal cannabinoid profiling revealed distinct exposure-history patterns for Δ9-THC and its major metabolites (**Fig. 2A**). Δ9-THC was significantly elevated after acute exposure in both females and males relative to vehicle (female, $P = 2.24 \times 10^{-3}$; male, $P = 3.78 \times 10^{-4}$), whereas repeated exposure showed greater variability and chronic exposure lower residual levels. In contrast, 11-hydroxy-Δ9-THC (H-Δ9-THC) was significantly elevated after both acute and repeated exposure in females ($P = 1.65 \times 10^{-2}$ and $P = 4.43 \times 10^{-2}$, respectively) and males ($P = 6.98 \times 10^{-7}$ and $P = 7.04 \times 10^{-3}$, respectively). 11-Nor-9-carboxy-Δ9-THC (C-Δ9-THC) showed greater accumulation in females, particularly after acute and repeated exposure, whereas levels in males were generally low or near the detection limit. Thus, H-Δ9-THC provided the most consistent exposure-associated signal across sexes, while C-Δ9-THC showed a more female-associated profile.

Multiblock PLS-DA of integrated untargeted and targeted lipidomics revealed exposure- and sex-associated organization of hippocampal lipid profiles (**Fig. 2B**). Acute and repeated THC samples separated from vehicle samples in the discriminant space, whereas chronic samples showed partial overlap. Loading-weight analyses identified phosphatidylethanolamine (PE) and

lysophosphatidylethanolamine (LPE) species as prominent contributors to component 1, with HexCer and SHexCer species contributing to component 2 (**Fig. S2C, D**). Targeted lipidomics further distinguished N-acylethanolamines (DEA, DHEA, SEA, and AEA) and PGE2, most abundant in vehicle samples, from PGF2α and 8-isoprostane, which were highest after chronic exposure. Differential lipid analyses identified distinct patterns across membrane-associated lipid classes (**Fig. 2C; Fig. S2A, B; Fig. S3**). PS species showed predominantly positive shifts across exposure contrasts, particularly in males after acute exposure and females after repeated and chronic exposure. PC species increased prominently in males after acute exposure, whereas O-PC and O-PE species showed progressively stronger negative shifts in females across repeated and chronic exposure, accompanied by increases in lysophospholipids. In males, O-PE decreases were most evident after acute exposure.

Sex-stratified differential abundance and UpSet analyses revealed distinct patterns in the extent and overlap of hippocampal lipid alterations (**Fig. 2D, E; Fig. S3**). Following acute exposure, both sexes showed decreased O-PE and increased PS and PE species, but the response was larger in males (176 versus 120 altered lipids). In males, the acute response included increased PC (24 species), LPE (18), and PS (17), together with decreased HexCer (20) and O-PE (15); 102 lipids increased and 74 decreased. In females, acute increases in PC and LPE were less extensive, while HexCer species changed in both directions. Female hippocampal lipid alterations increased from 120 after acute exposure to 148 after repeated and 204 after chronic exposure. Among the repeated and chronic contrasts, 64 lipids were shared exclusively between these comparisons and 62 were unique to chronic exposure, with both sets dominated by decreased O-PE species. Overall, 125 of 148 lipids altered after repeated exposure (84%) were also altered after chronic exposure. The female chronic response included decreased O-PE (54 species) and O-PC (14), together with increased PS (18), PC (16), and LPE (15) (**Fig. S3; Table S9**).

In contrast, males exhibited the largest number of altered lipids after acute exposure (176), with fewer after repeated (106) and chronic (76) exposure. Eighty-six lipids were unique to the acute contrast, and 47 of 106 repeated-exposure lipids (44%) were also altered after chronic exposure. Lipids shared across all three vehicle-referenced contrasts were enriched for PS species in both sexes. These findings indicate a broader and more persistent female hippocampal lipidomic signature across exposure histories, whereas the male response was predominantly acute in the age-adjusted analyses.

Because exposure history and life stage were linked by design, we assessed the robustness of these patterns with and without adjustment for chronological age (**Fig. S1B–E; Fig. S11, S12**). Unadjusted analyses preserved the progressive increase in altered hippocampal lipids in females (98, 135, and 192 after acute, repeated, and chronic exposure, respectively) and the larger male acute response relative to repeated exposure (238 versus 94 lipids). However, the male chronic-versus-vehicle contrast increased from 76 to 182 lipids without adjustment, indicating that the apparent

attenuation at the chronic stage was sensitive to age correction. Thus, age-adjusted results reflect lipidomic variation beyond a linear age trend, rather than age-independent THC effects, and the smaller chronic male response cannot be separated from age-associated variation.

Together, these findings reveal sex-divergent hippocampal lipidomic patterns across THC exposure histories. Females exhibited increasingly extensive and persistent changes involving ether-linked phospholipids, lysophospholipids, and PS species, whereas males showed a prominent acute response involving PC, LPE, PS, and glycosphingolipids. These patterns were accompanied by distinct cannabinoid-metabolite profiles and provide a basis for examining whether corresponding lipidomic signatures extend to the peripheral circulation.

THC Exposure Histories Reveal Sex-Divergent Circulating Lipid States and Compartment-Specific Network Organization

Having established sex-divergent hippocampal lipid remodeling across THC exposure histories, we next examined whether corresponding lipidomic patterns were present in the circulation or differed between compartments. Because serum was not available from vehicle-treated animals, circulating lipid profiles were compared across acute, repeated, and chronic THC-exposed groups rather than interpreted as THC-versus-vehicle effects. These comparisons therefore characterized exposure-history-associated circulating lipid states and their correspondence with hippocampal remodeling, while accounting for the confounding of exposure history with life stage.

Pairwise comparisons revealed substantial sex- and age-adjustment-dependent differences in circulating lipid profiles (**Fig. 3A; Fig. S4F, G; Fig. S12C**). Without adjustment, chronic-versus-acute comparisons identified 354 altered lipids in females and 292 in males, whereas chronic-versus-repeated comparisons identified 238 and 254, respectively. These responses primarily involved PC, SM, and TG species in females and TG and PC species in males. Following linear age adjustment, the chronic contrasts were markedly reduced (chronic versus acute: 51 females, 34 males; chronic versus repeated: 36 females, 71 males), while repeated versus acute became the largest contrast in both sexes (157 and 125 lipids, respectively). Within this adjusted comparison, females predominantly exhibited decreased TG species, whereas males showed decreased PE and ether-linked PE (O-PE) together with increased PC species. Importantly, because age and exposure history were aligned by design, linear adjustment largely removed differences between the youngest and oldest exposure groups, emphasizing deviations of the repeated group from that trend. Thus, adjusted contrasts captured nonlinear variation across exposure histories rather than age-independent THC effects.

The correspondence between circulating and hippocampal responses also depended on age adjustment (**Fig. 3A; Fig. S12B, C**). Without adjustment, chronic versus acute represented the largest comparison in both tissues and sexes, identifying 354 and 292 lipids in serum and 115 and 169 in the hippocampus of females and males, respectively. Following adjustment, repeated versus acute was

the largest contrast in female serum and hippocampus (157 and 101 lipids), whereas males showed the largest contrast between repeated and acute exposure in serum (125) but between chronic and acute exposure in hippocampus (135). Therefore, the relative magnitude of exposure-history contrasts across tissues was not robust to age adjustment and could not independently establish compartment-specific responses.

Additional analyses supported prominent sex-associated organization of the circulating lipidome (**Fig. S4**). Unsupervised PCA showed separation by sex primarily along PC2 (13% of variance), with more limited organization by exposure history (**Fig. S4A**). Serum cannabinoid profiling detected Δ9-THC, H-Δ9-THC, and C-Δ9-THC across THC-exposed groups (**Fig. S4B**). H-Δ9-THC and C-Δ9-THC were higher in females than males (two-way ANOVA, main effect of sex, $p < 0.001$ for both; no sex × exposure interaction), whereas Δ9-THC showed substantial overlap between sexes and exposure histories. Multiblock PLS-DA of stability-selected features further organized samples by exposure history, with acute and repeated groups occupying opposite regions and chronic samples intermediate (**Fig. S4C**). PC species were prominent contributors in the untargeted block, together with O-PE, TG, and SM features, whereas the targeted block included N-acylethanolamines and oxylipins (**Fig. S4D, E**).

Lipid Set Enrichment Analysis revealed distinct tissue- and sex-associated patterns (Fig. 3B). In female serum, repeated-versus-acute and chronic-versus-acute comparisons showed negative TG enrichment alongside positive PC and SM enrichment, whereas chronic versus repeated showed opposite TG and PC patterns. Male serum exhibited negative O-PE enrichment in repeated versus acute and positive enrichment in chronic versus repeated. In the chronic-versus-acute comparison, TG and SM enrichment also differed by sex, with positive TG and negative SM enrichment in males and the reverse pattern in females. These directional reversals were interpreted within the age-adjusted framework rather than as evidence of biological recovery, because the adjustment itself can generate opposing patterns between adjacent contrasts. Hippocampal enrichment profiles differed from serum, with limited TG and SM enrichment and stronger contributions from lysophospholipids, O-PE, and PS. In later exposure-history comparisons, females showed positive lysophospholipid and PS enrichment with negative O-PE enrichment, whereas males displayed the opposite directions. Thus, circulating lipid signatures preferentially involved neutral lipids and sphingomyelins, while hippocampal signatures emphasized sex-divergent remodeling of membrane-associated lipid pools.

Direct sex comparisons provided further evidence that circulating lipid differences were not fixed across exposure histories (**Fig. S5**). Within acute, repeated, and chronic groups, 196, 170, and 216 lipids differed between males and females, respectively, with comparable numbers showing higher abundance in either sex (**Fig. S5B, C**). Of 398 sex-differing lipids, 255 (64%) were identified in only one exposure history, whereas 41 differed across all three, nearly half of which were PC species (46%; **Fig. S5D**). TG species predominated among acute-specific differences, whereas SM, TG, and sterol-

related species were prominent in the chronic-specific set. Heatmap analyses similarly revealed changes spanning TG, PC, lysophospholipid, O-PE, SM, HexCer, and sterol-related classes (**Fig. S5A**). Although these comparisons cannot distinguish THC-associated differences from baseline sex differences or age-related effects in the absence of serum vehicle controls, their limited overlap indicated that the composition of sex-associated circulating lipid signatures varied across exposure histories.

We next examined whether these lipidomic patterns were accompanied by distinct cross-class correlation networks (**Fig. 3C, D**). Spearman networks were constructed separately by sex and tissue using stability-selected lipid features, retaining significant interclass correlations ($p < 0.05$) while excluding within-class associations. Serum networks prominently featured PC species and bioactive lipid mediators in both sexes, with additional TG representation in females and O-PE and ether-linked lysophospholipid features in males (**Fig. 3C**). Hippocampal networks in both sexes involved glycosphingolipids (HexCer and SHexCer) and oxylipins, whereas male networks additionally included PE, SM, PC, LNAPE, and N-acylethanolamine features (DEA and AEA), with more observed cross-class links (**Fig. 3D**). Because network size depended on stability-selected feature counts, these differences were interpreted descriptively rather than as formally established differences in network density or topology.

Metabolite–lipid correlations revealed additional sex- and compartment-specific associations (**Fig. 3C, D**). In female serum, Δ9-THC was inversely correlated with polyunsaturated phospholipids (PI 40:6, PC 40:8, and PC 20:4_22:6) and ether-linked lysophospholipids (LPE O-16:1 and LPE O-18:2). In male serum, C-Δ9-THC was positively associated with PE 34:2 and LPE O-16:0 but inversely associated with Cer 19:1;2O/24:0, SM 37:1;O2, and 13-KODE. In female hippocampus, Δ9-THC showed inverse associations with the annotated stearoyl ethanolamide-related feature and HexCer 18:1;2O/25:1;O. In males, very-long-chain (≥C22) glycosphingolipids were predominantly inversely associated with THC analytes, whereas HexCer 18:1;2O/18:0 showed a positive association. Polyunsaturated phospholipids, including PE 38:5 and PC 36:3, tended toward positive correlations, while oxylipins and N-acylethanolamines showed mixed associations. These findings identified distinct metabolite-associated lipid relationships across sex and tissue without establishing causal effects of individual THC metabolites.

Complementary network summaries and lipid-family analyses supported this compartment-specific organization (**Fig. S10**). Serum contained more significant cross-class lipid correlations than hippocampus, whereas hippocampal networks were smaller and more selective (**Fig. S10A**). Hippocampal choline-containing lipid classes (LPC, O-PC, and PC) showed weak, nonsignificant changes across exposure histories (**Fig. S10B**). In contrast, serum lipid-class sums and ratios revealed female-selective TG and LPC/PC changes, while TG-, lysophospholipid-, and O-PE-enriched serum modules showed sex-associated remodeling (**Fig. S10C–F**).

Together, these findings demonstrate that circulating lipidomic profiles differ by sex and THC exposure history but only partially parallel hippocampal remodeling. Sex-associated differences were evident within each exposure-history group and involved shifting lipid families, whereas comparisons across exposure histories remained sensitive to age adjustment. Serum responses preferentially involved TG, PC, SM, and ether-linked lipid classes, while hippocampal signatures emphasized membrane phospholipids and glycosphingolipids. Distinct metabolite–lipid correlation patterns further supported compartment-specific lipid-network organization, indicating that circulating lipidomics cannot be treated as a direct surrogate for hippocampal remodeling.

Stage-Resolved Brain–Serum Lipid Networks Reveal Sex-Divergent Integration of THC Metabolites

Having established sex-dependent lipid remodeling across individual lipid species, lipid classes, and tissues, we next asked whether these changes were organized into coordinated lipid modules. We applied consensus weighted correlation network analysis (WGCNA) to integrated untargeted and targeted lipidomics data, constructing separate networks for hippocampus and serum. Within each tissue, consensus modules were identified jointly across female and male datasets, defining lipid modules shared between sexes. Module eigengenes (MEs), calculated separately for each sex, provided quantitative summaries of module activity, allowing us to examine exposure-history-associated changes, relationships with cannabinoid metabolites, and coordination between hippocampal and circulating lipid states.

Consensus WGCNA identified 10 lipid modules in the hippocampus and 12 in serum (**Fig. S6, S7**). Modules varied in size and the proportion of highly connected hub lipids, with sex-associated differences in hub representation, indicating variation in internal module connectivity. Module overrepresentation analysis further revealed distinct but partially overlapping lipid architectures across tissues (**Fig. 4A, B**). Most modules were enriched for one or two lipid classes. In the hippocampus, these included a lysophospholipid/PS module (M1), two ether-linked phospholipid modules (M2, O-PC/O-PE; M5, O-PE), a glycosphingolipid module (M3, HexCer/TG), a sphingoid base-associated module (M4, SPB/Cer), and a PE-enriched module (M9). Serum modules encompassed a broader range of circulating lipid classes, including a TG-dominated module (M2), sphingolipid modules (M6, SPB; M10, SM), several lysophospholipid- and PC-enriched modules, and an O-PE module (M12). Ether-linked phospholipids and sphingolipids formed distinct modules in both tissues, whereas TG segregated into a dedicated serum module but clustered with HexCer in the hippocampus. Enrichment patterns were largely shared between sexes, as expected from the consensus network design, although enrichment strength differed.

We next examined which lipid modules varied across THC exposure histories (**Fig. 4C**). In the hippocampus, the lysophospholipid/PS-enriched M1 module showed significant exposure-associated variation in both sexes, identifying a shared membrane-associated response. In contrast, the O-PC/O-

PE-enriched M2 module varied significantly only in females, consistent with the extensive ether-linked phospholipid remodeling observed across later exposure histories. Serum module responses showed greater sex differentiation. Females exhibited significant changes in the TG-enriched M2 and lysophospholipid/PI-enriched M4 modules, whereas males showed significant changes in the PC-enriched M1, lysophospholipid/PC-enriched M5, and O-PE-enriched M12 modules. ME distributions across the broader module set confirmed that only selected modules showed pronounced exposure-associated shifts (**Fig. S8A–C**). Thus, exposure-history-associated variation was concentrated in specific lipid modules rather than uniformly distributed throughout the networks.

To examine broader coordination between hippocampal and circulating lipid modules, we integrated brain and serum MEs using DIABLO-based multiblock PLS-DA. Within each exposure history, females and males separated in the integrated space, although the pattern of separation differed across exposure histories (**Fig. 4D**). In contrast, exposure groups overlapped substantially within each sex. Female samples showed a loose ordering from acute to chronic exposure along the first averaged variate, whereas males showed no consistent ordering (**Fig. S8D**). Integrated brain–serum module profiles therefore distinguished sexes more clearly than exposure histories, with sex-associated organization varying across exposure stages.

We next examined stage-specific brain–serum module coupling and relationships with cannabinoid metabolites (**Fig. 4E; Fig. S9**). Within-tissue module correlations were observed across networks (dashed lines), whereas cross-tissue and module–THC correlations (solid lines) differed by exposure history and sex.

After acute exposure, males showed a limited number of cross-tissue correlations. Serum M1 (PC/Cer) and M11 (PL-rich) were positively correlated with brain M3 (HexCer/TG) and M4 (SPB/Cer/DG) ($r = 0.81–0.91$) and inversely correlated with brain M5 (O-PE) ($r = −0.90$ to $−0.91$), whereas THC analytes showed few prominent connections. In females, serum M6 (SPB/PC&SP) was positively correlated with brain lysophospholipid modules (M1, M8; $r = 0.84–0.86$) and inversely correlated with ether-linked phospholipid and PE modules (M2, M5, M9; $r = −0.82$ to $−0.91$). THC analytes were also integrated into the female network: C-Δ9-THC and H-Δ9-THC were correlated between brain and serum ($r = 0.86$ and 0.83, respectively), while brain Δ9-THC correlated with serum M4 ($r = 0.85$) and M11 ($r = −0.85$), and brain H-Δ9-THC correlated with serum M7 ($r = 0.86$) and M11 ($r = −0.85$).

After repeated exposure, serum M11 emerged as a prominent connecting module in males, correlating positively with brain M8 (LPC/LPI; $r = 0.99$) and inversely with brain M1, M2, and M9, representing lysophospholipid, ether-linked phospholipid, and PE-enriched modules ($r = −0.95$ to $−0.98$). Module–THC correlations remained limited. In females, inverse correlations between brain M3 (HexCer/TG) and serum M7–M9 (phospholipid- and lysophospholipid-enriched; $r = −0.90$ to $−0.93$) were accompanied by additional module–THC associations. Serum Δ9-THC correlated with brain M6

(PL/SP; r = 0.93) and M9 (PE; r = −0.91), whereas brain H-Δ9-THC correlated with serum M12 (O-PE; r = −0.91) and M3 (Cer/DG/TG/ChE; r = 0.90).

After chronic exposure, male networks exhibited the most extensive observed cross-tissue coupling. Brain M1 (LPC/LPE/PS) was inversely correlated with serum M12 (O-PE), M3 (Cer/DG/TG/ChE), and M4 (LPC/PI) (r = −0.86 to −0.91), while brain ether-linked phospholipid modules (M2, M5) correlated in opposite directions with serum M4 and M2 (TG) (|r| = 0.87–0.97). THC analytes also showed cross-tissue concordance: brain and serum Δ9-THC were positively correlated (r = 0.81), and serum H-Δ9-THC correlated positively with brain M9 (PE; r = 0.88). In contrast, female networks showed a more selective pattern, retaining coupling between brain M1 and serum M8 (LPC/PC/O-PE; r = 0.90). Brain Δ9-THC was also inversely correlated with serum M12 (O-PE), M10 (SM), and serum H-Δ9-THC (r = −0.88 to −0.90).

Together, these stage-specific networks revealed distinct patterns of brain–serum lipid coordination in females and males. Male networks showed limited cross-tissue coupling after acute exposure, prominent module-centered associations after repeated exposure, and more extensive observed coordination after chronic exposure, including concordant THC measurements across compartments. Female networks exhibited cannabinoid metabolite associations from the acute stage, followed by broader metabolite-associated relationships after repeated exposure and more selective coupling after chronic exposure. Because these networks were constructed from approximately five animals per sex and exposure history, the observed differences in connectivity and metabolite integration were interpreted descriptively rather than as formally established changes in network topology. Nevertheless, these patterns identify sex-associated differences in how coordinated lipid modules and individual THC analytes relate across central and circulating compartments.

Sex-Specific Brain–Serum Network Architectures Link THC Exposure to Divergent Membrane Lipid Remodeling.

Having defined stage-specific brain–serum coordination, we next asked whether females and males differed in the broader network architecture linking cannabinoid metabolism and lipid programs. To address this question, we constructed sex-specific networks integrating brain and serum module eigengenes with THC analytes across all exposure histories.

Both networks shared a core of highly connected brain modules, including M3 (HexCer/TG), M4 (SPB/Cer), and M5 (O-PE), but differed in their circulating hubs and connectivity with THC analytes (**Fig. 5A, B**). In females, THC analytes were associated with multiple brain and serum modules rather than a single dominant module, with numerous THC–THC and THC–module correlations (Fig. 5A). Female cross-tissue coupling was centered on serum M6 (SPB/PC&SP) and M3 (Cer/DG/TG/ChE), with serum M6 connected to brain ether-linked phospholipid, lysophospholipid/PS, and sphingolipid modules. In contrast, the male network showed a more module-centered organization (Fig. 5B). Brain

M2 (O-PC/O-PE) formed an additional hub, and the core brain modules (M2–M5) were connected to serum modules enriched for PC, TG, lysophospholipids, PI, SM, and ether-linked phospholipids. Male cross-tissue coupling was centered on serum M11 (PL-rich), consistent with its prominence after repeated exposure (**Fig. 4E**), whereas THC analytes occupied more peripheral positions with fewer significant module correlations. Because formal sex comparisons of network centrality and density were not performed, these architectural differences were interpreted descriptively rather than as quantitative differences in network topology.

Despite these differences, both networks retained a shared brain-module scaffold comprising ether-linked phospholipid, HexCer/TG, and Cer/SPB-associated programs. However, the circulating modules coupled to this scaffold differed between sexes. In males, the brain-module core was prominently associated with serum PC- and lysophospholipid-enriched modules, whereas in females it was connected more broadly with serum sphingoid base, triglyceride, and cannabinoid metabolite signals. Thus, similar lipid classes participated in distinct patterns of cross-compartment connectivity, suggesting that THC exposure history is associated with sex-divergent network organization rather than a single conserved lipidomic response.

Because ether-linked phospholipid modules were prominent in both networks (brain M5 in both sexes and brain M2 in males; **Fig. 5A, B**), we next examined the corresponding hippocampal lipid pools (**Fig. 5C**). In females, summed O-PE differed significantly across exposure groups (one-way ANOVA, $P = 0.006$), declining from vehicle through acute exposure to its lowest levels after repeated and chronic exposure. In contrast, summed LPE increased progressively ($P = 0.0014$), whereas PE remained unchanged ($P = 0.71$). In males, O-PE also differed across groups ($P = 0.004$), reaching its lowest levels after acute and repeated exposure. Male PE showed a nonsignificant tendency toward lower abundance across THC-exposed groups ($P = 0.086$), while LPE did not differ significantly ($P = 0.15$). Choline-containing lipid classes showed weaker patterns: LPC tended to parallel LPE (females, $P = 0.12$; males, $P = 0.20$), whereas O-PC and PC did not differ significantly ($P = 0.13$–0.72; **Fig. S10B**).

Structural mapping of O-PE species within brain modules M2 and M5 further resolved these changes (**Fig. 5D**). In females, fold changes were predominantly negative, particularly in the chronic-versus-acute comparison. In males, positive shifts predominated across all three comparisons and encompassed a broad range of chain lengths and unsaturation states. The LPE/O-PE ratio differed across exposure groups in both sexes but followed distinct trajectories (**Fig. 5E**). In females, this ratio increased progressively with exposure ($P = 0.0012$), whereas in males it increased after acute exposure and approached vehicle levels by chronic exposure ($P = 0.041$). Similarly, the LPE/PE ratio increased in females ($P = 0.038$) but did not differ significantly in males ($P = 0.15$). These ratios reflect the relative balance between lysophospholipid and phospholipid pools rather than directly measuring membrane lipid flux or turnover. The class-level patterns were similar with and without age adjustment

(**Fig. S13**), supporting more sustained membrane-associated lipid alterations in females and a distinct male response that approached vehicle levels at the chronic stage.

Structural maps of the LPE/PS axis within brain M1 showed that sex-associated remodeling extended beyond ether-linked phospholipids (**Fig. 5F**). In females, LPE- and PS-related species were predominantly increased in the chronic-versus-acute and repeated-versus-acute comparisons, whereas in males these species were predominantly decreased across all three comparisons. Consistent with these patterns, summed hippocampal PS differed significantly across exposure groups in females ($P = 0.013$) but not in males ($P = 0.22$; **Fig. 5C**). Together, these findings connect the sex-divergent network architectures with distinct membrane lipid signatures, characterized by broader lysophospholipid and PS-associated remodeling in females and a more restricted class-level response in males.

We next examined whether these hippocampal signatures were reflected in corresponding serum lipid pools (**Fig. S10**). Because serum was unavailable from vehicle-treated animals, these analyses compared lipid profiles across THC exposure histories rather than against a vehicle reference. Most serum lipid-class sums, including LPC, LPE, and DG, did not differ significantly ($P = 0.22–0.94$; **Fig. S10D**). In females, however, serum TG ($P = 0.016$; **Fig. S10D**) and the LPC/PC ratio ($P = 0.046$; **Fig. S10C**) were highest after acute exposure and lower after repeated and chronic exposure. Structural mapping of the TG-enriched serum M2 module showed that this response extended across multiple TG species, most of which declined from acute to repeated and chronic exposure, with a partial increase between repeated and chronic exposure (**Fig. S10F**). In males, TG species within M2 tended to increase from repeated to chronic exposure, consistent with the nonsignificant trend in summed TG ($P = 0.20$). Because DG abundance did not differ significantly in either sex, the female tendency toward an increased DG/TG ratio after repeated and chronic exposure ($P = 0.061$) was consistent with lower TG rather than higher DG abundance. Thus, while hippocampal LPE/O-PE and LPE/PE ratios increased across exposure histories in females, the circulating LPC/PC ratio was highest after acute exposure and subsequently declined, indicating that central remodeling was not directly mirrored in serum. In males, serum O-PE tended to decline after repeated exposure and approach earlier levels after chronic exposure ($P = 0.071$; **Fig. S10D**), consistent with decreases in O-PE species from acute to repeated exposure within serum M12 (**Fig. S10E**). Serum LPE/O-PE ratios (females, $P = 0.61$; males, $P = 0.31$) and DG/TG ratios (females, $P = 0.061$; males, $P = 0.14$) did not differ significantly across exposure histories (**Fig. S10C**).

Together, these findings reveal sex-divergent lipid adaptations associated with THC exposure history. Females exhibited a network in which cannabinoid analytes were broadly associated with brain and serum lipid modules, accompanied by sustained reductions in hippocampal ether-linked phospholipids and increases in lysophospholipids. Males showed a more module-centered network involving brain ether-linked phospholipid and sphingolipid modules and a prominent serum

phospholipid hub, with hippocampal O-PE reductions most evident after acute and repeated exposure. By linking network architecture with distinct membrane lipid trajectories, these results suggest that biological sex is associated not only with the extent and persistence of lipidomic remodeling, but also with the broader organization of lipid relationships across brain and peripheral circulation.

Discussion:

Our findings suggest that repeated THC exposure is not represented in the lipidome as a single, uniform biochemical signature. Rather, distinct exposure histories were associated with lipid states that differed by biological sex, tissue compartment, and cannabinoid-metabolite context. Across analyses spanning individual lipid species, lipid classes, coordinated lipid modules, and integrated brain–serum networks, females showed a more persistent hippocampal lipid response in which THC analytes were broadly connected to lipid modules, whereas males showed an acute-biased hippocampal response that was followed by progressively broader brain–serum coordination. Collectively, these observations support a framework in which biological sex influences not only the magnitude of THC-associated lipid remodeling, but also the systems-level architecture through which prior cannabinoid exposure becomes embedded across central and circulating metabolic networks.

A central premise of this study was that THC exposure history represents a biologically meaningful dimension of cannabinoid response that cannot be captured by an acute exposure model alone. Human cannabis use follows heterogeneous longitudinal trajectories, including limited or intermittent use, recurrent exposure, sustained use, and declining patterns across adulthood, rather than a single uniform course (22, 23). These trajectories are unfolding within a broader context of increasing adult cannabis use and rapidly changing patterns of access and consumption (1). Although no experimental paradigm can reproduce the full complexity of human cannabis use, the life-stage-resolved vapor design allowed us to examine whether successive THC exposure epochs are associated with transient, re-exposure-related, or progressively reorganized metabolic states. Cannabinoid measurements provided an important biochemical dimension to this framework. In brain, Δ9-THC and H-Δ9-THC were detected in both sexes, whereas C-Δ9-THC showed preferentially greater abundance in females. In serum, H-Δ9-THC and C-Δ9-THC were higher in females than in males regardless of exposure history, whereas Δ9-THC did not differ by sex. This pattern is consistent with established evidence that THC is highly lipophilic and that its pharmacokinetics, tissue distribution, and metabolite profiles can vary according to sex and age (2, 5-7). Parent THC and its hydroxylated and carboxylated metabolites should therefore not be viewed as interchangeable measures of exposure burden; rather, each may reflect a partially distinct combination of recent exposure, metabolic conversion, distribution, and tissue persistence. Consistent with this interpretation, lipid associations were organized around specific THC analytes rather than a single aggregate cannabinoid signal, suggesting that metabolite context constitutes an additional dimension through which exposure history becomes biologically embedded.

The hippocampus provides a particularly informative compartment for examining THC-associated lipid remodeling because it integrates cannabinoid signaling, CB1 receptor-mediated synaptic regulation, and cognitive processes that are highly sensitive to THC exposure (24-26). Within this compartment, THC exposure history was associated with remodeling across multiple interconnected lipid systems, including phospholipids, lysophospholipids, ether-linked phospholipids, sphingolipids, glycosphingolipids, neutral lipids, and bioactive lipid mediators, which together contribute to membrane organization, phospholipid remodeling, vesicular biology, lipid raft architecture, redox buffering, stress-responsive signaling, and the partitioning of lipophilic molecules within biological membranes (12, 14, 15). A particularly striking feature of the hippocampal response was its temporal divergence between females and males. Females developed progressively larger and more persistent lipid remodeling across repeated and chronic exposure histories, whereas males exhibited a stronger acute response. The male response after chronic exposure was smaller only after age adjustment and therefore could not be separated from age-associated remodeling. These findings suggest sustained membrane-associated remodeling in females and an acute-dominant response in males.

Across differential abundance, enrichment, structural mapping, and ratio analyses, females showed a progressive decline in O-PE together with increases in LPE and in LPE/O-PE and LPE/PE ratios across exposure histories, and O-PE species within ether-linked phospholipid modules shifted predominantly negatively. In males, O-PE was reduced after acute and repeated exposure but returned toward vehicle levels after chronic exposure, the LPE/O-PE ratio increased transiently after acute exposure, and O-PE species shifted positively in later age-adjusted exposure comparisons. These class-level patterns were similar with and without age adjustment in both sexes (**Fig. S13**). Lysophospholipid and PS species in the lysophospholipid/PS module also shifted in opposite directions between sexes. These observations are consistent with a working model in which female remodeling involves a sustained shift from ether-linked phospholipids toward lysophospholipids, whereas in males the class-level O-PE and LPE changes were transient and returned toward vehicle levels by chronic exposure. Although this interpretation remains inferential because lipid turnover, phospholipase activity, and ether-lipid biosynthetic flux were not directly measured, it is supported by the established biological functions of ether-linked phospholipids and plasmalogens in membrane architecture, vesicular trafficking, lipid microdomain organization, cellular signaling, and protection against oxidative stress (12, 13). Accordingly, the O-PE/LPE axis may serve as a sensitive readout of cannabinoid-associated membrane remodeling.

HexCer/TG- and SPB/Cer-enriched brain modules were among the most highly connected modules in both female and male networks, defining a shared brain core together with ether-linked phospholipid modules. The two sexes differed not in the presence of this core but in its circulating partners: in females it was coupled primarily to sphingoid base- and neutral-lipid-enriched serum

modules, and in males to a phospholipid-enriched serum hub. At the species level, very-long-chain glycosphingolipids in the male hippocampus were predominantly inversely correlated with THC analytes, whereas a shorter-chain HexCer species showed the opposite association, suggesting that chain-length-specific glycosphingolipid composition may be sensitive to cannabinoid exposure. Because sphingolipids and glycosphingolipids organize neural membrane microdomains and contribute to receptor clustering and stress-responsive signaling (14, 27), these patterns suggest distinct sex-dependent strategies of membrane adaptation: a module-coordinated, cross-compartment architecture in males and a distributed, metabolite-integrated architecture in females. These correlational networks do not establish causal regulation of sphingolipid pathways but provide testable hypotheses for how sex shapes membrane organization and brain–peripheral metabolic coupling across THC exposure history.

Serum lipidomics reflected THC exposure history, but did not mirror hippocampal lipid remodeling. Circulating lipid profiles integrate lipid transport, lipoprotein-associated lipid exchange, hepatic and peripheral lipid handling, and systemic metabolic state, whereas hippocampal lipidomics reflects more compartment-specific membrane and signaling changes (28, 29). Consistent with this distinction, serum modules spanned broader phospholipid, neutral-lipid, and sterol pools than brain modules, female serum responses were dominated by TG-associated systemic remodeling, and male serum responses involved ether-linked phospholipid (O-PE) and PC-enriched modules that shifted transiently across exposure history. Serum exposure-history contrasts were sensitive to age adjustment: without adjustment, contrasts involving chronic exposure were largest, whereas after adjustment repeated-versus-acute differences predominated (**Fig. S12**). In contrast, sex differences within each exposure history were extensive and did not depend on cross-age comparison. Serum also showed extensive sex differences within every exposure history, but only a small core of lipids differed by sex across all three, indicating that most sex differences in the circulating lipidome varied with exposure history rather than reflecting fixed sexual dimorphism. Despite these compartmental differences, brain and serum lipid modules were coupled in a sex- and exposure-dependent manner.

The network analyses moved the study beyond differential lipid abundance to reveal how THC exposure history becomes organized across coordinated lipid programs. This distinction is important because lipid species do not function as independent biochemical endpoints; they are linked through shared biosynthesis, membrane localization, remodeling, transport, and degradation, making lipidomics particularly well suited to systems-level analysis (15). Consensus WGCNA grouped covarying lipids into modules shared by both sexes within each tissue and summarized their coordinated behavior through module eigengenes (18). The sex divergence we observed therefore reflects differences in how the same lipid programs responded and were coupled, rather than differences in network composition. Within this framework, exposure history acted on a limited set of coordinated programs rather than reorganizing the lipidome globally. Exposure sensitivity was

concentrated in membrane lysophospholipid and ether-linked phospholipid programs in the hippocampus, and in sex-specific circulating programs: triglyceride and lysophospholipid modules in females, and PC and ether-linked phospholipid modules in males (**Fig. 4C**). This selectivity suggests that exposure history is encoded preferentially in lipid pools that undergo active remodeling, rather than in the bulk structural lipidome. More striking was the sex divergence in how these programs were coupled across compartments. In males, brain and serum modules became progressively more coordinated, and parent THC corresponded across tissues after chronic exposure, consistent with greater cross-compartment coordination at later exposure histories. In females, chronic exposure was instead accompanied by an inverse relationship between brain Δ9-THC and circulating H-Δ9-THC. Because THC is highly lipophilic and accumulates in tissue (2), and its disposition differs by sex (5, 6), prolonged exposure may uncouple central parent-compound burden from peripheral metabolite levels in females. If confirmed, this would mean that circulating cannabinoid and lipid measures index brain exposure differently in females and males, with direct relevance to biomarker development. These stage-stratified associations were derived from small groups and require validation. Nevertheless, stability-selected modules were associated with different THC analytes in females and males, and brain and serum module eigengenes were coordinated in a sex-dependent manner (Fig. 4E). These findings support a model in which exposure history is reflected in sex-specific coordination of lipid modules across compartments rather than in a single dominant lipid signature.

Collectively, our findings support two distinct patterns through which females and males respond to THC exposure history, consistent with growing evidence that cannabinoid responses differ between sexes through interacting pharmacological, endocrine, and biological mechanisms (4). In females, hippocampal remodeling expanded and persisted across exposure histories, a pattern observed with and without age adjustment (**Fig. S12, S13**), and centered on a shift from ether-linked phospholipids toward lysophospholipids, reflected in decreased O-PE and increased LPE and in higher LPE/O-PE and LPE/PE ratios. Because phospholipid remodeling influences membrane composition and biophysical properties, and ether-linked phospholipids contribute to membrane organization and redox-sensitive lipid biology, these observations raise the possibility that female THC adaptation is characterized by sustained membrane-associated remodeling rather than a transient shift in lipid abundance alone (13, 30). By contrast, males exhibited a more pronounced acute hippocampal lipidomic response, whereas later exposure histories were characterized by broader coordination among brain and circulating lipid modules. Whether the number of altered lipids declines at chronic exposure in males could not be determined independently of age. The mechanisms underlying these sex-specific adaptive states remain unresolved because lipid flux, phospholipase activity, ether-lipid biosynthesis, sphingolipid metabolism, and cannabinoid-metabolizing enzyme activity were not directly measured. Future studies integrating lipidomics with metabolic flux analysis, enzymatic measurements, and spatially or cell-type-resolved approaches will be important for

determining whether these coordinated network states represent causal mechanisms of adaptation or molecular correlates of repeated THC exposure history.

The serum arm of the study addressed a complementary biological question that extended, rather than replicated, the vehicle-controlled hippocampal analysis. The repeated-vehicle hippocampal cohort established a procedural reference for defining central lipid remodeling, whereas serum lipidomics was designed to determine whether distinct THC exposure histories generate separable circulating metabolic states and whether those states converge with or diverge from central lipid remodeling. Accordingly, the serum findings should be interpreted as comparisons among exposure-history states rather than as conventional baseline-normalized THC-versus-vehicle contrasts. This distinction strengthens the interpretation of serum lipidomics as a peripheral readout of systemic adaptation while clearly defining the biological question addressed by the circulating compartment. Future studies incorporating age-matched serum vehicle groups across all exposure stages will be important for distinguishing the relative contributions of THC exposure itself, normal aging, repeated vapor exposure, and their interactions across tissues and biological compartments.

An important feature of this study is that age and exposure history were intentionally integrated rather than experimentally dissociated. The acute, repeated, and chronic paradigms were designed to represent biologically distinct histories of cannabinoid exposure unfolding across the lifespan rather than simple differences in cumulative THC dose. This distinction is biologically meaningful because the endocannabinoid system undergoes age-dependent remodeling, and accumulating evidence indicates that both endogenous cannabinoid signaling and the biological consequences of THC exposure vary across the lifespan (31). Consistent with this concept, chronic low-dose THC produces age-dependent cognitive and molecular effects in mice, improving cognitive performance and partially restoring age-associated molecular signatures in older animals rather than acting uniformly across ages (32). Recent human studies likewise suggest that endocannabinoid tone differs across age groups and can be modified by cannabis exposure, further supporting the concept that cannabinoid responses are interpreted within an age-dependent biological context (33). Accordingly, our objective was not to model age-independent cannabinoid pharmacology, but rather to determine how distinct life-stage exposure histories become biologically embedded. To reduce the contribution of chronological age to exposure-focused comparisons, age was modeled as a continuous covariate and its linear effect was removed before lipidomic analyses while preserving sex-associated biological variation. This adjustment substantially attenuated age-associated lipidomic structure in both brain and serum, providing a more conservative basis for interpreting the remaining lipidomic variation in relation to exposure history. However, linear adjustment applied to three age levels that coincide with exposure groups largely removes differences between the youngest and oldest groups, so results were compared with unadjusted analyses. The age-matched repeated-THC versus repeated-vehicle comparison, the progressive female hippocampal response, the acute-dominant male response, and

the class-level O-PE/LPE patterns were observed in both analyses (**Fig. S12, S13**), whereas contrasts involving chronic exposure, particularly in serum, depended on the adjustment. Future factorial studies incorporating age-matched vehicle cohorts at each exposure stage will be valuable for further disentangling the respective contributions of aging, repeated exposure, and cumulative cannabinoid history.

Several limitations should be considered when interpreting these findings. Although the lipidomic and network analyses identified coordinated molecular states associated with THC exposure history, they do not establish causal relationships between cannabinoid metabolites, lipid modules, and downstream biological outcomes. Likewise, although targeted cannabinoid metabolites were quantified directly, the enzymatic processes governing sex-dependent differences in metabolite abundance, including cannabinoid-metabolizing enzyme activity, tissue-specific disposition, and metabolic flux, were not measured (3). In addition, lipidomics provides molecular resolution without identifying the cellular origin of individual lipid signatures. Consequently, the observed remodeling likely reflects integrated contributions from multiple hippocampal and peripheral cell populations, including neurons, astrocytes, microglia, oligodendrocytes, endothelial cells, and peripheral metabolic tissues. Furthermore, the present study focused primarily on molecular adaptation rather than directly assessing the behavioral, electrophysiological, vascular, or inflammatory consequences of the identified lipid-network states. Finally, although WGCNA and multiblock integration provide powerful systems-level approaches for identifying coordinated lipid architecture, module organization and network relationships remain dependent on cohort size and analytical parameters and therefore should be interpreted as coordinated biological states rather than fixed mechanistic pathways (18). These limitations also define important opportunities for future investigation. Integrating lipidomics with metabolic flux analysis, enzymatic measurements, stable-isotope tracing, spatial lipidomics, and cell-type-resolved approaches will be important for determining whether the coordinated lipid-network states identified here represent causal mechanisms of adaptation or molecular correlates of repeated THC exposure history.

Within these boundaries, our findings provide an integrated framework for understanding how THC exposure history becomes biologically embedded across central and circulating lipid systems. Rather than identifying a single cannabinoid-associated lipid signature, this study demonstrates that repeated THC exposure leads to the emergence of sex-specific adaptive metabolic states organized by coordinated lipid-network remodeling. Across multiple complementary analytical levels, from cannabinoid-metabolite profiling and lipid-class remodeling to brain–serum network integration, we consistently observed that females developed a more persistent, metabolite-integrated pattern of lipid adaptation, whereas males exhibited a more acute-biased response followed by broader coordination among brain and circulating lipid modules. These findings suggest that biological sex influences not only the magnitude and persistence of THC-associated lipid remodeling, but also the systems-level

architecture through which cannabinoid metabolites become integrated into adaptive membrane and metabolic networks. More broadly, this work supports the concept that repeated cannabinoid exposure should not be viewed simply as a sequence of transient pharmacological events. Instead, exposure history itself emerges as a biologically meaningful determinant of adaptive metabolic organization across the lifespan. By shifting attention from individual lipid alterations toward coordinated lipid-network architecture and adaptive metabolic states, our findings suggest that THC exposure history constitutes a biologically meaningful organizing principle in cannabinoid biology.

Competing Interests

The authors declare no competing interests.

Acknowledgments

This work was supported by research grants from the South Carolina Alzheimer's Disease Research Center (ADRC) Pilot Grant, the COBRE in Neurodevelopment and Its Disorders P20GM148302 Research Grant, MUSC Specialized Center of Research Excellence (SCORE) 2U54DA016511 to L.K., C.L., R.M.P., and O.A.; and R01NS147071-01A1 Research Grants to O.A.

Author Contributions

C.C., L.K., K.S., R.M.P., and O.A. designed the research; C.C., L.K., C.L., X.G., and S.W. performed the research; C.C. and L.K. analyzed the data; and C.C., R.M.P., and O.A. wrote the paper.

Data Availability

All data are included in the manuscript.

Code Availability

All code used in this study was cited and described within the manuscript. Details of the code implementation, including algorithms and data processing scripts, are provided in the methods section and relevant figure legends.

Figure 1. Repeated THC vapor exposure establishes sex-divergent brain cannabinoid metabolite states and coordinated lipidomic remodeling.

(A) Experimental design of the longitudinal THC vapor exposure paradigm. Rats were exposed during young adulthood, middle adulthood, and/or aged adulthood using a forced-vapor paradigm consisting of five trials per day, two 3-s puffs per trial, for 20 days, with THC administered at 100 mg/mL. Tissues were collected at the indicated time points for lipidomic analyses.

(B) Targeted quantification of Δ9-THC and its metabolites, 11-hydroxy-Δ9-THC (H-Δ9-THC) and 11-nor-9-carboxy-Δ9-THC (C-Δ9-THC), in the repeated THC and repeated vehicle groups, stratified by

sex. Boxplots show the median and interquartile range, and individual points represent individual animals. Statistical significance was assessed across the four groups by two-way ANOVA (sex × exposure group) followed by Tukey's HSD post hoc test. Exact P values are shown for significant comparisons only ($P < 0.05$); comparisons without a P value were not significant. n = 5–6 animals per group.

(C) Multivariate analysis of the targeted and untargeted brain lipidomics datasets. Unsupervised principal component analysis is shown on the left. On the right, the two lipidomics datasets were integrated as separate data blocks using the DIABLO framework implemented in the mixOmics R package to identify correlated and discriminative lipid signatures. The resulting averaged component plot shows lipidomic organization according to THC exposure and sex.

(D-E) Loading weights of the features with the largest absolute loadings on components 1 and 2 of the multiblock PLS-DA (DIABLO) model, shown for the untargeted lipidomics block (**D**; top 15 lipid species) and the targeted lipidomics block (**E**; bioactive lipid mediators). Bar fill indicates the exposure group (repeated THC or vehicle) and bar outline indicates the sex of the group with the highest median abundance of each feature. Colored tiles along the y-axis denote lipid class.

(F) Circos plot of lipid features selected by the multiblock PLS-DA (DIABLO) model. The outer track indicates lipid class. The inner heatmap rings show Spearman correlations of each lipid with Δ9-THC, H-Δ9-THC, and C-Δ9-THC; all coefficients are shown regardless of significance. Connecting lines show lipid–lipid Spearman correlations with $P < 0.05$ and $|\rho| > 0.6$ (red, positive; green, inverse). Correlations were calculated across repeated THC and Vehicle animals (n = 5-6).

Figure 2. THC exposure history produces sex-divergent hippocampal cannabinoid profiles and coordinated lipidomic remodeling.

(A) Hippocampal concentrations of C-Δ9-THC, Δ9-THC, and H-Δ9-THC across vehicle, acute, repeated, and chronic THC exposure groups, stratified by sex. Boxplots show the median (center line), interquartile range (box), and 1.5 × IQR (whiskers); individual points represent biological replicates. Statistical significance was assessed across the eight groups by two-way ANOVA (sex × exposure group) followed by Tukey's HSD post hoc test. Exact P values are shown for significant comparisons only ($P < 0.05$); comparisons without a P value were not significant. n = 5–6 animals per group.

(B) Multivariate analysis of integrated targeted and untargeted hippocampal lipidomics using the DIABLO framework implemented in the mixOmics R package. Targeted and untargeted lipidomics datasets were analyzed as separate data blocks to identify correlated and discriminative lipid signatures across exposure groups. The resulting partial least squares discriminant analysis (multiblock PLS-DA) averaged component plot illustrates lipidomic organization according to THC exposure history and sex. Triangles (blue) and circles (pink) represent males and females,

respectively, whereas point colors denote exposure groups. Dashed ellipses indicate group-level clustering.

(C) Heatmap of log2 fold changes for all detected lipid species across vehicle-referenced exposure comparisons, stratified by sex. Rows represent lipid classes (including NAE, Lyso-PL, Oxy, PC, PE, PG, PI, PS, O-PC, O-PE, LNAPE, SPB, Cer, HexCer, SM, ST/ChE, DG, TG, and Others), and columns represent experimental comparisons. Red indicates increased abundance and blue indicates decreased abundance relative to vehicle controls; the color scale is capped at ± 4.

(D–E) UpSet plots summarizing significantly altered lipid species ($P < 0.05$) across vehicle-referenced exposure comparisons in females **(D)** and males **(E)**. Vertical bars indicate the number of shared significant lipids within each intersection, with stacked colors representing lipid-class composition. The dot matrix identifies the corresponding comparison sets. Horizontal bars summarize the total number of significantly altered lipids in each comparison, with red indicating increased and blue indicating decreased lipid abundance.

Figure 3. THC exposure history generates sex-dependent circulating lipid states that partially converge with brain lipid remodeling.

(A) UpSet plots summarizing significantly altered lipids ($P < 0.05$) in pairwise comparisons among exposure histories (repeated vs acute, chronic vs repeated, chronic vs acute), in serum (left) and hippocampus (right) of females (upper) and males (lower). Female samples are shown in the upper panels and male samples in the lower panels; serum is shown on the left and brain on the right. Vertical bars indicate the number of significantly altered lipids within each intersection, with stacked colors representing lipid classes. The dot matrix defines the corresponding comparison sets. Horizontal bars summarize the total number of significantly altered lipids for each comparison, with red indicating increased and blue indicating decreased lipid abundance.

(B) Lipid Set Enrichment Analysis (LSEA) of serum (left) and brain (right) lipidomes. Circle color represents the normalized enrichment score (NES), ranging from −4 (blue) to 4 (red). Circle size corresponds to $-\log_{10}$(P value). White backgrounds indicate statistically significant enrichment ($P < 0.05$), whereas gray backgrounds indicate non-significant enrichment.

(C–D) Circos plots of correlation networks in serum (**C**) and hippocampus (**D**) of females (upper) and males (lower). Features were selected by elastic-net stability selection and integrated by multiblock PLS-DA (DIABLO) separately for each tissue and sex (see Methods); selected features therefore differ between panels. The outer ring indicates lipid class. Inner heatmap tracks show Spearman correlations between each feature and C-Δ9-THC, H-Δ9-THC, and Δ9-THC (red, positive; blue, inverse), with asterisks indicating $P < 0.05$. Connecting lines show lipid–lipid Spearman correlations with $P < 0.05$ and $|\rho| > 0.6$ (red, positive; green, inverse) excluding within-class links. P values are unadjusted. n = 5–6 animals per group.

Figure 4. Stage-resolved lipid network analysis reveals sex-dependent brain–serum module coordination across THC exposure history.

(A–B) Overrepresentation analysis of WGCNA-derived lipid modules in brain **(A)** and serum **(B)**, stratified by sex. Columns represent lipid modules and rows represent lipid classes. Circle color indicates fold enrichment, with warmer colors representing greater enrichment. Only positive enrichment was evaluated using a one-sided Fisher's exact test. Enrichment was computed on sex-specific module members with significant module membership (MM > 0.6; P < 0.05). Symbol size reflects statistical significance based on FDR-adjusted P values. Female and male results are indicated by pink circles and blue triangles, respectively.

(C) Module eigengene (ME) distributions across THC exposure histories, stratified by tissue and sex. Hippocampal analyses include vehicle, acute, repeated, and chronic groups, whereas serum analyses include acute, repeated, and chronic exposure groups. Only modules showing significant exposure-associated differences in at least one sex are displayed. Boxplots represent module eigengene values, and P values were obtained using Kruskal–Wallis tests.

(D) DIABLO-based multiblock integration of hippocampal and serum module eigengenes, shown separately in each THC exposure history. Shape indicates sex (blue triangles, male; pink circles, female) and color indicates exposure history. Averaged variates 1 and 2 summarize coordinated cross-tissue lipid-module organization.

(E) Circos plots of significant Pearson correlations (P < 0.05, unadjusted) among hippocampal modules, serum modules, and THC analytes (Δ9-THC, H-Δ9-THC, and C-Δ9-THC) at acute, repeated, and chronic exposure stages. Female networks are shown in the upper row and male networks in the lower row (n = 5–6 animals per network). Only modules and analytes with at least one significant correlation are shown, so the nodes differ between networks. The inner ring indicates tissue (dark brown, hippocampus; light brown, serum), and the outer ring indicates module color as in (**A–B**). Solid lines show cross-tissue correlations and dashed lines within-tissue correlations; line color indicates correlation direction and strength (red, positive; blue, inverse). Module labels give each module's dominant lipid classes from overrepresentation analysis (A–B). Because overrepresentation was assessed among lipids with significant module membership (MM) in each sex, labels for some consensus modules differ slightly between females and males, although module composition is identical (Tables S11–S12).

Figure 5. Sex-specific lipid-network architecture links THC exposure history to divergent membrane remodeling programs.

(A–B) Network visualization of significant correlations among WGCNA-derived lipid modules and THC metabolites in females **(A)** and males **(B)**. Nodes represent brain (circles) and serum (triangles) lipid modules or THC-related analytes. Node size indicates hub centrality, with larger nodes representing

the five highest-ranked hubs within each network. Connecting lines represent correlations; solid lines indicate $P < 0.05$ and dashed lines indicate nonsignificant trends. Red lines indicate positive correlations and blue lines indicate inverse correlations, with color intensity corresponding to correlation strength. Module labels correspond to WGCNA module identities.

(C) Summed relative abundance of LPE, O-PE, PE, and PS species in the hippocampus of repeated vehicle (Veh), acute, repeated, and chronic groups, stratified by sex. Each species was normalized before summation, so values reflect the average relative level of species within each class.

(D) Structural maps of O-PE species within the hippocampal O-PC/O-PE (M2) and O-PE (M5) modules in females (upper) and males (lower) for chronic vs acute, chronic vs repeated, and repeated vs acute comparisons. The x-axis represents total fatty-acyl chain length and the y-axis represents the total number of double bonds. Individual lipid species are colored according to log fold change, with red indicating increased and blue indicating decreased abundance.

(E) Ratio of summed relative abundance of LPE/O-PE and LPE/PE across vehicle, acute, repeated, and chronic THC exposure conditions, stratified by sex.

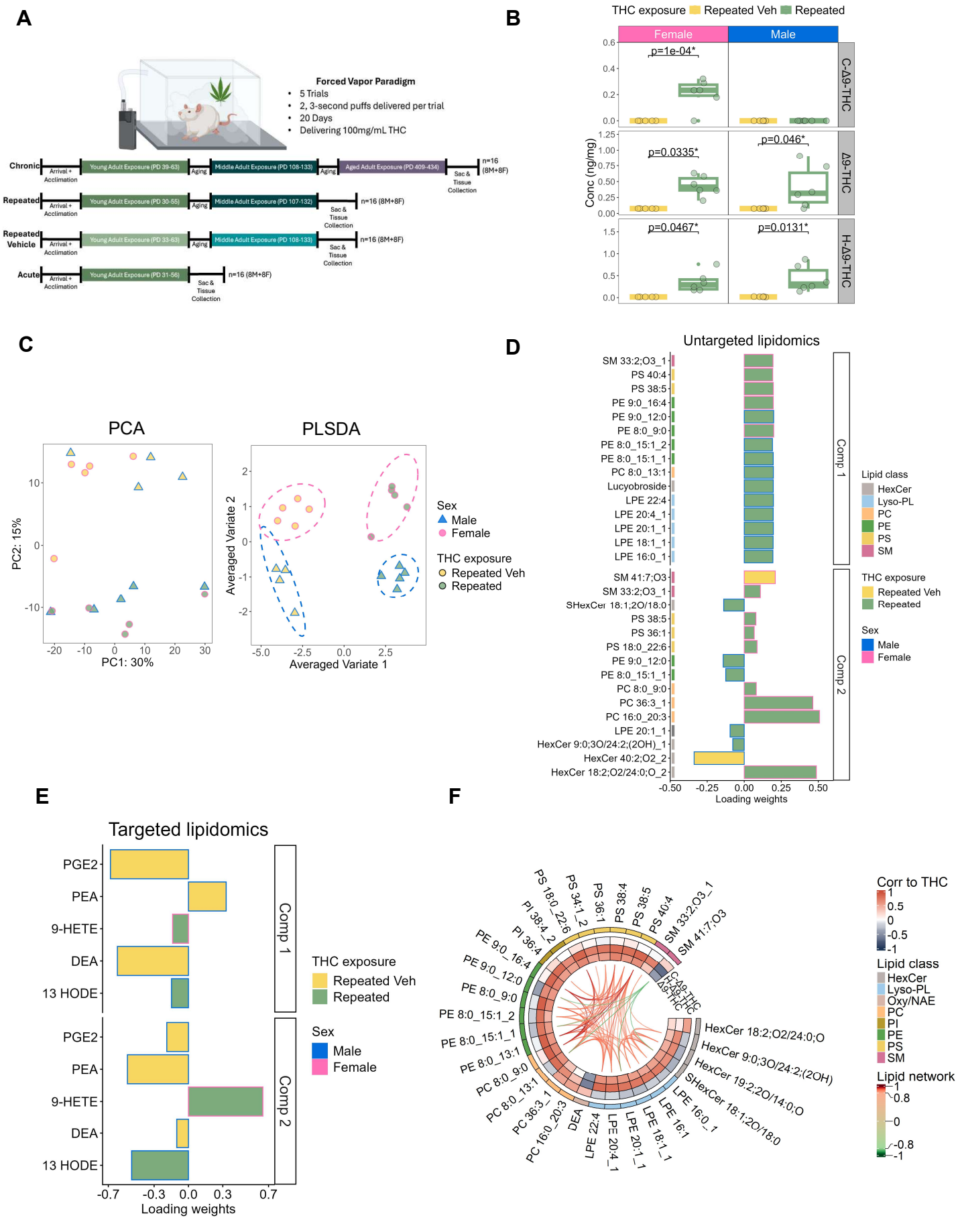
(F) Structural maps of LPE and PS species within the hippocampal lysophospholipid/PS module (M1) in females (upper) and males (lower). Axes, comparisons, and color coding are as in (**D**).

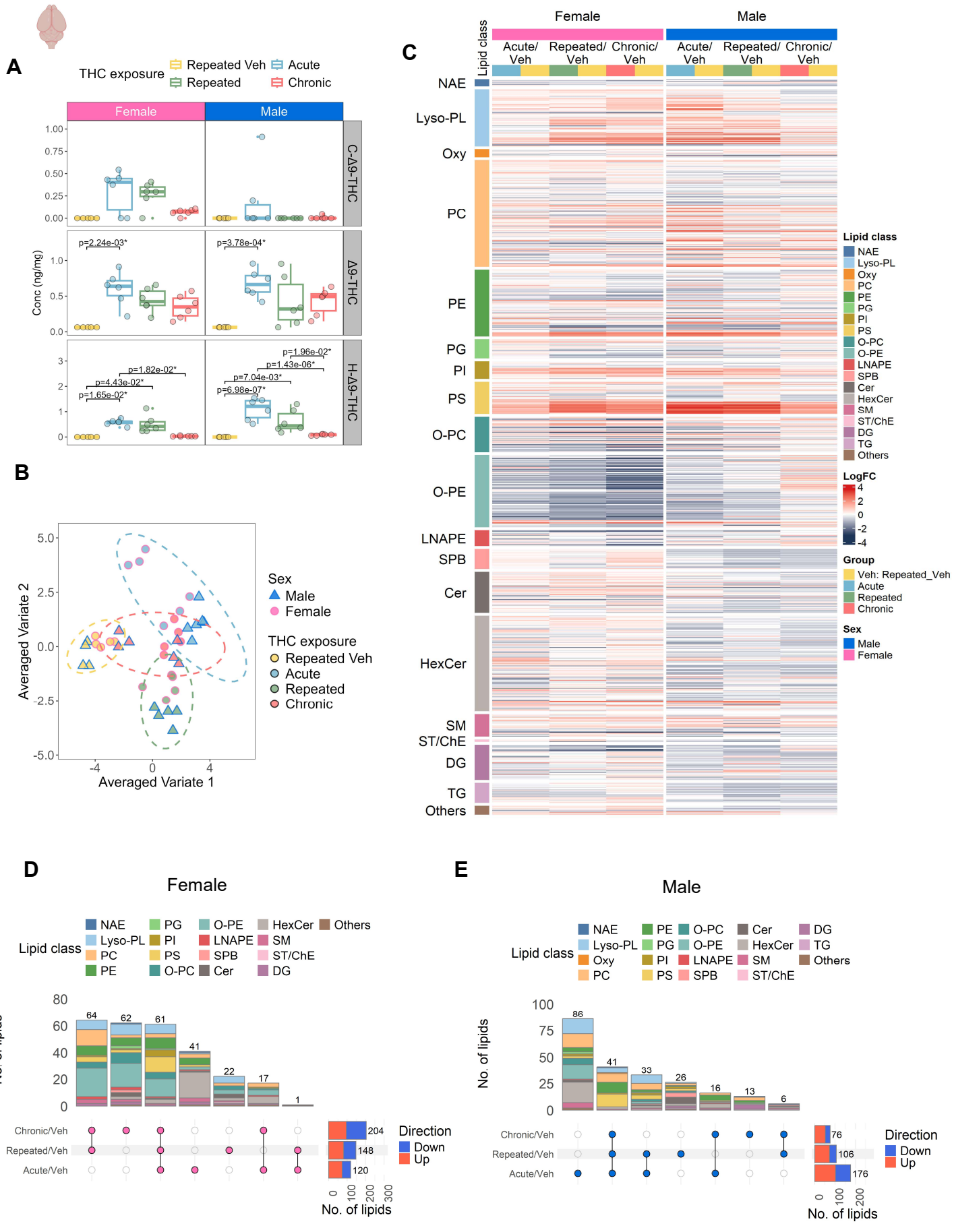
In (**C**) and (**E**), boxplots show the median and interquartile range with whiskers extending to 1.5 × IQR, and points represent individual animals (n = 5–6 per group). P values are from one-way ANOVA across the four exposure groups within each sex. LPE, lysophosphatidylethanolamine; O-PE, ether-linked phosphatidylethanolamine; PE, phosphatidylethanolamine; PS, phosphatidylserine.

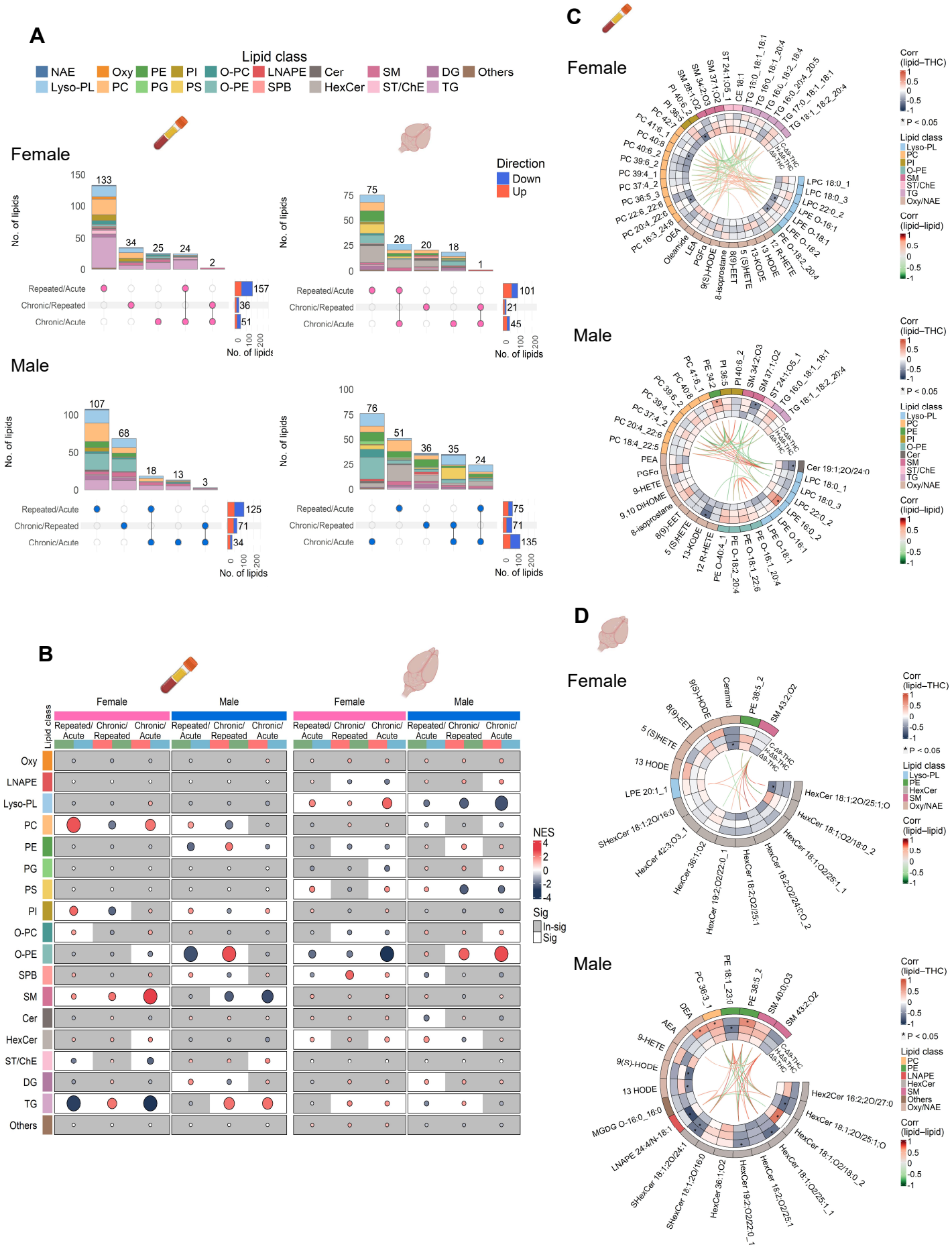
Reference

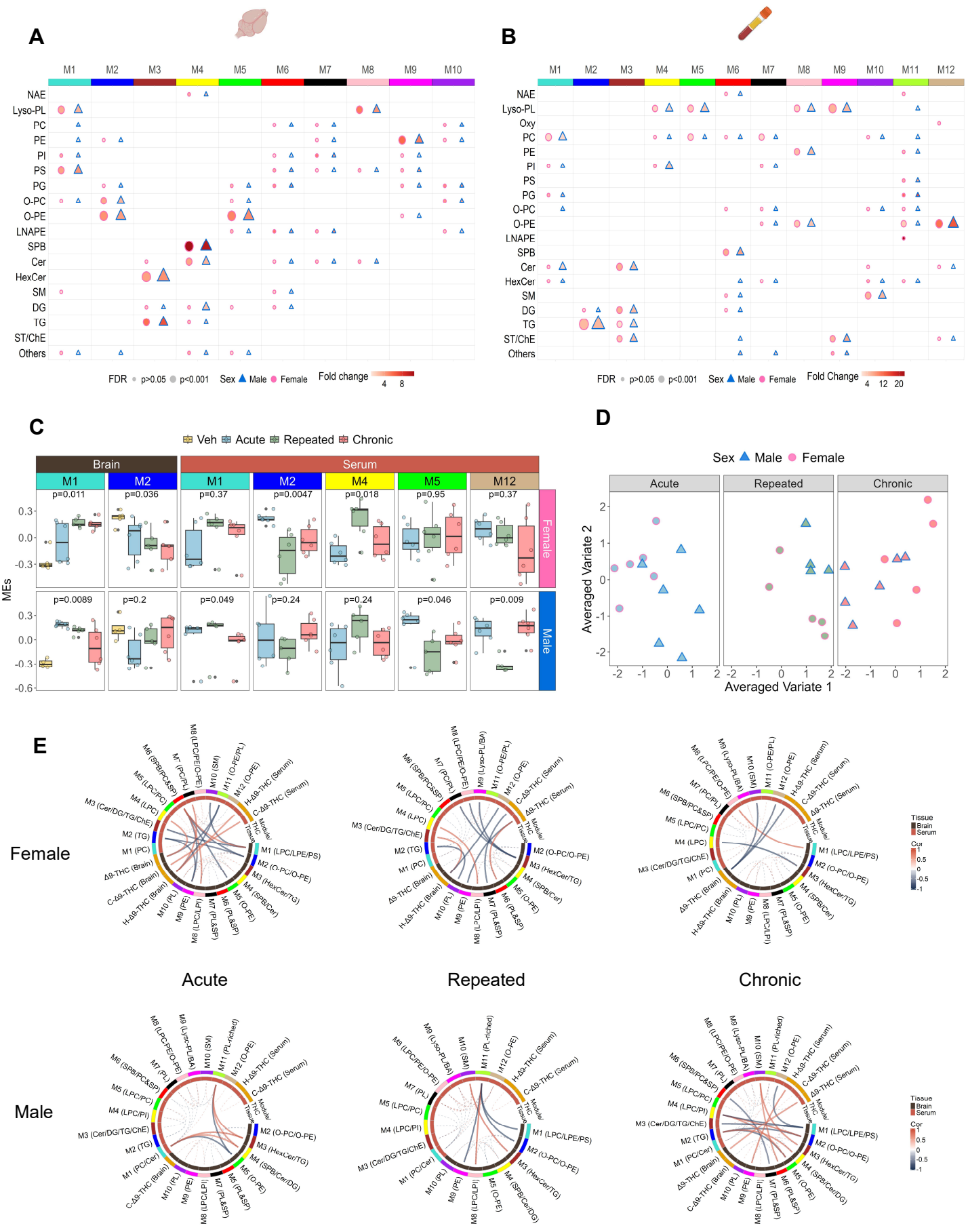
1. D. Hasin, C. Walsh, Trends over time in adult cannabis use: A review of recent findings. *Curr Opin Psychol* **38**, 80-85 (2021).
2. M. A. Huestis, Human cannabinoid pharmacokinetics. *Chem Biodivers* **4**, 1770-1804 (2007).
3. K. C. B. Yabut, Y. Winnie Wen, K. T. Simon, N. Isoherranen, CYP2C9, CYP3A and CYP2C19 metabolize Delta9-tetrahydrocannabinol to multiple metabolites but metabolism is affected by human liver fatty acid binding protein (FABP1). *Biochem Pharmacol* **228**, 116191 (2024).
4. Z. D. Cooper, R. M. Craft, Sex-Dependent Effects of Cannabis and Cannabinoids: A Translational Perspective. *Neuropsychopharmacology* **43**, 34-51 (2018).
5. J. L. Wiley, J. J. Burston, Sex differences in Delta(9)-tetrahydrocannabinol metabolism and in vivo pharmacology following acute and repeated dosing in adolescent rats. *Neurosci Lett* **576**, 51-55 (2014).
6. A. Torrens *et al.*, Comparative Pharmacokinetics of Delta(9)-Tetrahydrocannabinol in Adolescent and Adult Male and Female Rats. *Cannabis Cannabinoid Res* **7**, 814-826 (2022).
7. N. A. Sallam *et al.*, Sex Differences in Plasma, Adipose Tissue, and Central Accumulation of Cannabinoids, and Behavioral Effects of Oral Cannabis Consumption in Male and Female C57BL/6 Mice. *Int J Neuropsychopharmacol* **26**, 773-783 (2023).
8. D. Piomelli, The molecular logic of endocannabinoid signalling. *Nat Rev Neurosci* **4**, 873-884 (2003).

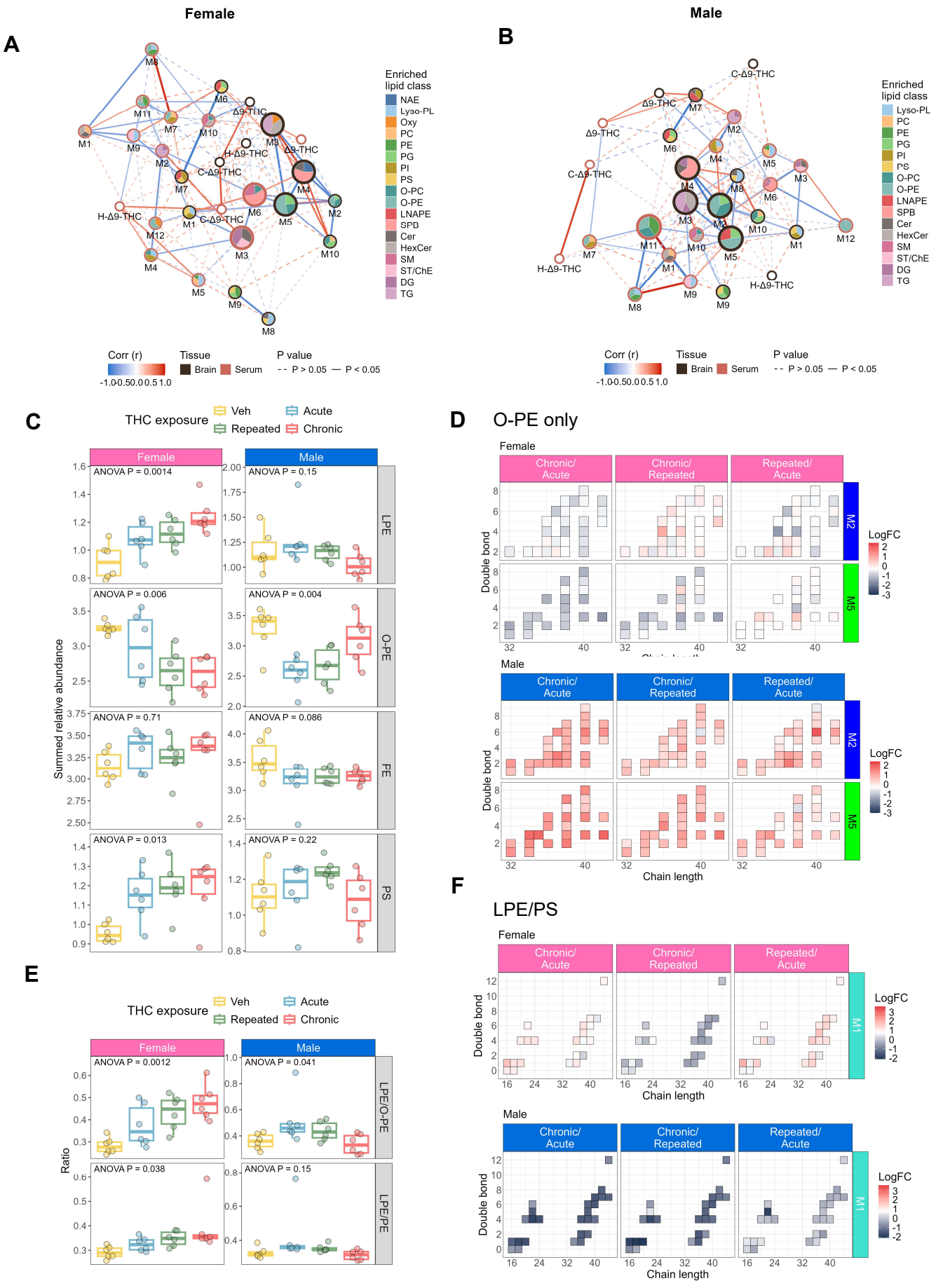
9. K. Tsuboi, T. Uyama, Y. Okamoto, N. Ueda, Endocannabinoids and related N-acylethanolamines: biological activities and metabolism. *Inflamm Regen* **38**, 28 (2018).
10. N. Murataeva, A. Straiker, K. Mackie, Parsing the players: 2-arachidonoylglycerol synthesis and degradation in the CNS. *Br J Pharmacol* **171**, 1379-1391 (2014).
11. G. Astarita, J. Geaga, F. Ahmed, D. Piomelli, Targeted lipidomics as a tool to investigate endocannabinoid function. *Int Rev Neurobiol* **85**, 35-55 (2009).
12. N. E. Braverman, A. B. Moser, Functions of plasmalogen lipids in health and disease. *Biochim Biophys Acta* **1822**, 1442-1452 (2012).
13. F. Dorninger, S. Forss-Petter, I. Wimmer, J. Berger, Plasmalogens, platelet-activating factor and beyond - Ether lipids in signaling and neurodegeneration. *Neurobiol Dis* **145**, 105061 (2020).
14. Y. Zhang, X. Li, K. A. Becker, E. Gulbins, Ceramide-enriched membrane domains--structure and function. *Biochim Biophys Acta* **1788**, 178-183 (2009).
15. R. W. Gross, X. Han, Lipidomics at the interface of structure and function in systems biology. *Chem Biol* **18**, 284-291 (2011).
16. M. A. Alves *et al.*, Systems biology approaches to study lipidomes in health and disease. *Biochim Biophys Acta Mol Cell Biol Lipids* **1866**, 158857 (2021).
17. M. E. Ritchie *et al.*, limma powers differential expression analyses for RNA-sequencing and microarray studies. *Nucleic Acids Res* **43**, e47 (2015).
18. P. Langfelder, S. Horvath, WGCNA: an R package for weighted correlation network analysis. *BMC Bioinformatics* **9**, 559 (2008).
19. J. Friedman, T. Hastie, R. Tibshirani, Regularization Paths for Generalized Linear Models via Coordinate Descent. *J Stat Softw* **33**, 1-22 (2010).
20. F. Rohart, B. Gautier, A. Singh, L. C. KA, mixOmics: An R package for 'omics feature selection and multiple data integration. *PLoS Comput Biol* **13**, e1005752 (2017).
21. G. Korotkevich *et al.*, Fast gene set enrichment analysis. *bioRxiv* 10.1101/060012, 060012 (2021).
22. Y. M. Terry-McElrath *et al.*, Longitudinal patterns of marijuana use across ages 18-50 in a US national sample: A descriptive examination of predictors and health correlates of repeated measures latent class membership. *Drug Alcohol Depend* **171**, 70-83 (2017).
23. A. R. Mahar, M. P. Bancks, S. Sidney, J. Reis, G. L. Kinney, Trajectory modeling of cannabis use over 30 years identifies five unique longitudinal patterns. *Sci Rep* **13**, 23070 (2023).
24. L. E. Wise, A. J. Thorpe, A. H. Lichtman, Hippocampal CB(1) receptors mediate the memory impairing effects of Delta(9)-tetrahydrocannabinol. *Neuropsychopharmacology* **34**, 2072-2080 (2009).
25. I. Katona, T. F. Freund, Multiple functions of endocannabinoid signaling in the brain. *Annu Rev Neurosci* **35**, 529-558 (2012).
26. P. E. Castillo, T. J. Younts, A. E. Chavez, Y. Hashimotodani, Endocannabinoid signaling and synaptic function. *Neuron* **76**, 70-81 (2012).
27. A. S. B. Olsen, N. J. Faergeman, Sphingolipids: membrane microdomains in brain development, function and neurological diseases. *Open Biol* **7** (2017).
28. O. Quehenberger *et al.*, Lipidomics reveals a remarkable diversity of lipids in human plasma. *J Lipid Res* **51**, 3299-3305 (2010).
29. J. H. Yoon *et al.*, Brain lipidomics: From functional landscape to clinical significance. *Sci Adv* **8**, eadc9317 (2022).
30. B. Wang, P. Tontonoz, Phospholipid Remodeling in Physiology and Disease. *Annu Rev Physiol* **81**, 165-188 (2019).
31. A. Bilkei-Gorzo, The endocannabinoid system in normal and pathological brain ageing. *Philos Trans R Soc Lond B Biol Sci* **367**, 3326-3341 (2012).
32. A. Bilkei-Gorzo *et al.*, A chronic low dose of Delta(9)-tetrahydrocannabinol (THC) restores cognitive function in old mice. *Nat Med* **23**, 782-787 (2017).
33. A. W. J. Morris *et al.*, Age differences in endocannabinoid tone are ameliorated after recent cannabis use. *Sci Rep* **16**, 3483 (2026).


A
Forced Vapor Paradigm
5 Trials
2, 3-second puffs delivered per trial
20 Days
Delivering 100mg/mL THC
Chronic
Arrival + Acclimation
Young Adult Exposure (PD 39-63)
Aging
Middle Adult Exposure (PD 108-133)
Aging
Aged Adult Exposure (PD 409-434)
Sac & Tissue Collection
n=16 (8M+8F)
Repeated
Young Adult Exposure (PD 30-55)
Middle Adult Exposure (PD 107-132)
Repeated Vehicle
Young Adult Exposure (PD 33-63)
Middle Adult Exposure (PD 108-133)
Acute
Young Adult Exposure (PD 31-56)
B
THC exposure
Repeated Veh
Repeated
Female
Male
C-Δ9-THC
Δ9-THC
H-Δ9-THC
Conc (ng/mg)
p=1e-04*
p=0.0335*
p=0.046*
p=0.0467*
p=0.0131*
C
PCA
PLSDA
PC2: 15%
PC1: 30%
Averaged Variate 2
Averaged Variate 1
Sex
Male
Female
THC exposure
Repeated Veh
Repeated
D
Untargeted lipidomics
SM 33:2;O3_1
PS 40:4
PS 38:5
PE 9:0_16:4
PE 9:0_12:0
PE 8:0_9:0
PE 8:0_15:1_2
PE 8:0_15:1_1
PC 8:0_13:1
Lucyobroside
LPE 22:4
LPE 20:4_1
LPE 20:1_1
LPE 18:1_1
LPE 16:0_1
SM 41:7;O3
SHexCer 18:1;2O/18:0
PS 36:1
PS 18:0_22:6
HexCer 9:0;3O/24:2;(2OH)_1
HexCer 40:2;O2_2
HexCer 18:2;O2/24:0;O_2
Comp 1
Comp 2
Loading weights
Lipid class
HexCer
Lyso-PL
PC
PE
PS
SM
THC exposure
Repeated Veh
Repeated
Sex
Male
Female
E
Targeted lipidomics
PGE2
PEA
9-HETE
DEA
13 HODE
Comp 1
Comp 2
Loading weights
THC exposure
Repeated Veh
Repeated
Sex
Male
Female
F
PS 18:0_22:6
PS 34:1_2
PS 36:1
PS 38:4
PS 38:5
PS 40:4
SM 33:2;O3_1
SM 41:7;O3
PI 38:4_2
PI 36:4
PE 9:0_16:4
PE 9:0_12:0
PE 8:0_9:0
PE 8:0_15:1_2
PE 8:0_15:1_1
PE 8:0_13:1
PC 8:0_9:0
PC 8:0_13:1
PC 36:3_1
PC 16:0_20:3
DEA
LPE 22:4
LPE 20:4_1
LPE 20:1_1
LPE 18:1_1
LPE 16:1
LPE 16:0_1
SHexCer 18:1;2O/18:0
HexCer 19:2;2O/14:0;O
HexCer 9:0;3O/24:2;(2OH)
HexCer 18:2;O2/24:0;O
C-Δ9-THC
H-Δ9-THC
Δ9-THC
Corr to THC
1
0.5
0
-0.5
-1
Lipid class
HexCer
Lyso-PL
Oxy/NAE
PC
PI
PE
PS
SM
Lipid network
1
0.8
0
-0.8
-1


A
THC exposure
Repeated Veh
Acute
Repeated
Chronic
Female
Male
C-Δ9-THC
Δ9-THC
H-Δ9-THC
Conc (ng/mg)
p=2.24e-03*
p=3.78e-04*
p=1.82e-02*
p=4.43e-02*
p=1.65e-02*
p=1.96e-02*
p=1.43e-06*
p=7.04e-03*
p=6.98e-07*
B
Averaged Variate 1
Averaged Variate 2
Sex
Male
Female
THC exposure
Repeated Veh
Acute
Repeated
Chronic
C
Lipid class
Acute/ Veh
Repeated/ Veh
Chronic/ Veh
NAE
Lyso-PL
Oxy
PC
PE
PG
PI
PS
O-PC
O-PE
LNAPE
SPB
Cer
HexCer
SM
ST/ChE
DG
TG
Others
LogFC
Group
Veh: Repeated_Veh
Acute
Repeated
Chronic
Sex
Male
Female
D
Female
Lipid class
No. of lipids
Chronic/Veh
Repeated/Veh
Acute/Veh
Direction
Down
Up
E
Male
Lipid class
No. of lipids
Chronic/Veh
Repeated/Veh
Acute/Veh
Direction
Down
Up


A
Lipid class
NAE
Oxy
PE
PI
O-PC
LNAPE
Cer
SM
DG
Others
Lyso-PL
PC
PG
PS
O-PE
SPB
HexCer
ST/ChE
TG
Female
Direction
Down
Up
No. of lipids
Repeated/Acute
Chronic/Repeated
Chronic/Acute
Male
B
Female
Male
Lipid class
Repeated/ Acute
Chronic/ Repeated
Chronic/ Acute
Oxy
LNAPE
Lyso-PL
PC
PE
PG
PS
PI
O-PC
O-PE
SPB
SM
Cer
HexCer
ST/ChE
DG
TG
Others
NES
Sig
In-sig
Sig
C
Female
Male
Corr (lipid–THC)
* P < 0.05
Lipid class
Corr (lipid–lipid)
D
Female
Male


A
M1 M2 M3 M4 M5 M6 M7 M8 M9 M10
NAE
Lyso-PL
PC
PE
PI
PS
PG
O-PC
O-PE
LNAPE
SPB
Cer
HexCer
SM
DG
TG
ST/ChE
Others
FDR p>0.05 p<0.001 Sex Male Female Fold change 4 8
B
M1 M2 M3 M4 M5 M6 M7 M8 M9 M10 M11 M12
NAE
Lyso-PL
Oxy
PC
PE
PI
PS
PG
O-PC
O-PE
LNAPE
SPB
Cer
HexCer
SM
DG
TG
ST/ChE
Others
FDR p>0.05 p<0.001 Sex Male Female Fold Change 4 12 20
C
Veh Acute Repeated Chronic
Brain
Serum
M1 M2 M1 M2 M4 M5 M12
p=0.011 p=0.036 p=0.37 p=0.0047 p=0.018 p=0.95 p=0.37
Female
p=0.0089 p=0.2 p=0.049 p=0.24 p=0.24 p=0.046 p=0.009
Male
MEs
D
Sex Male Female
Acute Repeated Chronic
Averaged Variate 2
Averaged Variate 1
E
Female
Acute
Repeated
Chronic
Male
Tissue Brain Serum
Cor 1 0.5 0 -0.5 -1


A
Female
Enriched lipid class
NAE
Lyso-PL
Oxy
PC
PE
PG
PI
PS
O-PC
O-PE
LNAPE
SPB
Cer
HexCer
SM
ST/ChE
DG
TG
Corr (r)
-1.0 -0.5 0.0 0.5 1.0
Tissue
Brain
Serum
P value
P > 0.05
P < 0.05
B
Male
C
THC exposure
Veh
Acute
Repeated
Chronic
Female
Male
ANOVA P = 0.0014
ANOVA P = 0.15
ANOVA P = 0.006
ANOVA P = 0.004
ANOVA P = 0.71
ANOVA P = 0.086
ANOVA P = 0.013
ANOVA P = 0.22
LPE
O-PE
PE
PS
Summed relative abundance
D
O-PE only
Chronic/ Acute
Chronic/ Repeated
Repeated/ Acute
Double bond
Chain length
LogFC
E
ANOVA P = 0.0012
ANOVA P = 0.041
ANOVA P = 0.038
ANOVA P = 0.15
LPE/O-PE
LPE/PE
Ratio
F
LPE/PS

Supplementary Files

This is a list of supplementary files associated with this preprint. Click to download.

- Supplementaryinformation.pdf